DEIF, A. S. (1982). *Advanced Matrix Theory for Scientists and Engineers*, p. 113. Tunbridge Wells/London: Abacus Press; New York/Toronto: Halstead Press Division, John Wiley.
DORSET, D. L. (1993). *MSA Bull.* **23**, 99–108.
DORSET, D. L., KOPP, S., FRYER, J. R. & TIVOL, W. F. (1995). *Ultramicroscopy*, **57**, 59–89.
DORSET, D. L., TIVOL, W. F. & TURNER, J. N. (1991). *Ultramicroscopy*, **38**, 41–45.
DORSET, D. L., TIVOL, W. F. & TURNER, J. N. (1992). *Acta Cryst.* A**48**, 562–568.
DORSET, D. L., TIVOL, W. F. & TURNER, J. N. (1993). *J. Appl. Cryst.* **26**, 778–786.
FUJIMOTO, F. (1959). *J. Phys. Soc. Jpn*, **14**, 1558–1568.
GERBER, R. B. & KARPLUS, M. (1972). *J. Chem. Phys.* **56**, 1921–1936.
GLUSKER, J. P. (1993). Editor. *Acta Cryst.* D**49**, 1–222.
HIRSCH, P. B., HOWIE, A., NICHOLSON, R. B., PASHLEY, D. W. & WHELAN, M. J. (1965). *Electron Microscopy of Thin Crystals*, 1st ed. New York: Plenum Press; London: Butterworths.
LADD, M. F. C. & PALMER, R. A. (1980). *Theory and Practice of Direct Methods in Crystallography*, edited by M. F. C. LADD & R. A. PALMER, pp. 93–150. New York/London: Plenum Press.
LIPSON, H. & COCHRAN, W. (1966). *The Determination of Crystal Structures*, p. 246. London: G. Bell.
MARTIN, A. (1969). *Nuovo Cimento*, A**59**, 131–152.
MERZBACHER, E. (1961). *Quantum Mechanics*, pp. 153–154, 222. New York/London: John Wiley.
MISHNEV, A. F. (1991). *Direct Methods of Solving Crystal Structures*, edited by H. SCHENK, pp. 399–400. New York/London: Plenum Press.
MISHNEV, A. F. & BELYAKOV, S. V. (1992). *Acta Cryst.* A**48**, 260–263.
MISHNEV, A. F. & SHVETS, A. E. (1979). *Sov. Phys. Crystallogr.* **24**, 13–15.
NEWTON, R. G. (1968). *J. Math. Phys.* **9**, 2050–2055.
NEWTON, R. G. (1982). *Scattering Theory of Waves and Particles*, 2nd ed., pp. 191–195. New York/Heidelberg/Berlin: Springer-Verlag.
PENG, L.-M. & WANG, S. Q. (1994). *Acta Cryst.* A**50**, 759–771.
SAKURAI, J. J. (1967). *Advanced Quantum Mechanics*, pp. 185–188. Reading, MA/Menlo Park, CA/London/Don Mills, ON: Addison Wesley.
SAYRE, D. (1952). *Acta Cryst.* **5**, 60–65.
SPENCE, J. (1995). Personal communication.
STURKEY, L. (1962). *Proc. Phys. Soc. London*, **80**, 321–354.
TIVOL, W. F., DORSET, D. L., MCCOURT, M. P. & TURNER, J. N. (1993). *MSA Bull.* **23**, 91–98.

Acta Cryst. (1995). A**51**, 716–739

Equilibrium Morphology of Incommensurately Modulated Crystals: a Superspace Description

BY M. KREMERS, H. MEEKES, P. BENNEMA AND M. A. VERHEIJEN

RIM Laboratory of Solid State Chemistry, University of Nijmegen, Toernooiveld, 6525 ED Nijmegen, The Netherlands

AND J. P. VAN DER EERDEN

Interfaces and Thermodynamics, University of Utrecht, 3508 TB Utrecht, The Netherlands

(*Received* 11 *November* 1994; *accepted* 16 *March* 1995)

Abstract

The theory for the explanation of equilibrium morphologies of incommensurately modulated one-dimensional crystals, presented in a previous paper, is extended to the case of incommensurately modulated three-dimensional crystals. It is shown that, concerning the morphology, there exists a one-to-one correspondence between faces on the physical crystal and crystallographic hyperplanes of the embedded crystal in superspace. This holds for both main faces and satellite faces. The occurrence of the latter, however, is unique for incommensurately modulated crystals. It is shown that the stability of satellite faces, as well as main faces, can be attributed to a principle of selective cuts. The superspace approach that is developed leads to a calculation method for surface free energies that, in principle, can be applied to incommensurately modulated structures of arbitrary complexity. Equilibrium morphologies are constructed from the calculated surface free energies by means of a standard Wulff plot. The dependence of the equilibrium morphology on several structural parameters is studied for an incommensurately modulated simple cubic model crystal. This study allows for a basic understanding of the differences in morphology of $AuTe_2$ crystals and $[(CH_3)_4N]_2ZnCl_4$ crystals.

1. Introduction

It is well known that the morphology of crystals is often determined by flat faces. The orientation of these faces is related to directions of Fourier wave vectors of the structure; the Fourier wave vectors are parallel to the face normals. Crystal faces can be labelled perfectly by a set of three integral indices because the Fourier wave vectors of a classical crystal build a three-dimensional lattice. In incommensurately modulated crystals, it is not possible

to describe all Fourier wave vectors by an integral linear combination of three basis vectors. Instead, the Fourier wave vectors build a $\mathbb{Z}$-module with a rank higher than its dimension (Janner & Janssen, 1977; de Wolff, Janssen & Janner 1981). The rank determines the number of rationally independent Fourier wave vectors. This number can exceed the dimension whenever the structure can be considered to be a deformed classical crystal in which the wavelengths of the deformations are incommensurate with the underlying basic lattice. The difference between the rank and the dimension gives the number of independent modulations that are present. A famous example is the mineral calaverite $Au_{1-x}Ag_xTe_2$. Its complex morphology has puzzled crystallographers for a long time (see, for example, Goldschmidt, Palache & Peacock, 1931). A labelling of the crystal faces by three low indices did not seem to be possible, although many attempts were made. At present, it is known that there is a one-dimensional incommensurate modulation in this crystal (Sueno, Kimata & Ohmasa, 1979; Van Tendeloo, Gregoriades & Amelinckx, 1983; Schutte & de Boer, 1988), so that the rank of the $\mathbb{Z}$-module is four. The Fourier wave vectors, therefore, can be labelled by four integral indices. This was the key to solving the only partly understood morphology of $Au_{1-x}Ag_xTe_2$ crystals. The faces that determine the morphology of incommensurately modulated crystals are perpendicular to Fourier wave vectors of the $\mathbb{Z}$-module. It was shown that the faces of $Au_{1-x}Ag_xTe_2$ could be labelled, very satisfactorily, with four low integral indices (Dam, Janner & Donnay, 1985; Janner & Dam, 1989). The same behaviour has been found for many other incommensurately modulated crystals (see Bennema *et al.*, 1991). In Fig. 1, the result, as was given by Janner & Dam (1989), is reproduced for a typical twin crystal of $Au_{1-x}Ag_xTe_2$. A crystal face is called a main face if the fourth index is zero. Otherwise, it is called a satellite face. The investigation of many mineral crystals, but also of crystals grown in our laboratory, has revealed that satellite faces are very dominant for the morphology of $Au_{1-x}Ag_xTe_2$ crystals. This is a clear example of a strong influence of the incommensurate modulation on the physical properties of a crystal. The beautiful description of the orientation of crystal faces, however, does not yet clarify the nature of this influence. In order to have a better understanding, one would also like to be able to explain the stability of these faces. It is shown in this paper that it is not expected, in advance, that satellite faces can appear as stable crystal faces. In this paper, we take on the challenge to find an explanation for the stability of (satellite) faces on incommensurately modulated crystals using a superspace approach.

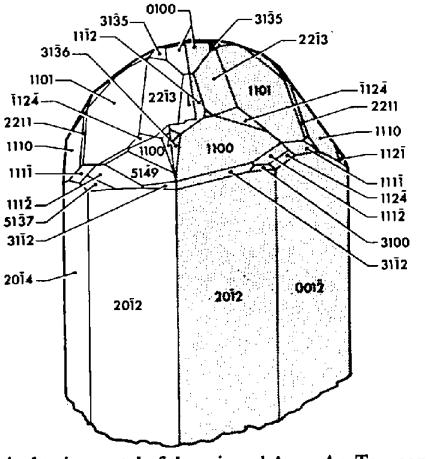

Fig. 1. A typical twin crystal of the mineral $Au_{1-x}Ag_xTe_2$, consisting of two individuals. This figure was reproduced from Janner & Dam (1989). The crystal faces are labelled with four integral indices, reflecting the presence of an incommensurate modulation. The faces with a non-zero fourth index are called satellite faces. It is clear that many large satellite faces determine the morphology of $Au_{1-x}Ag_xTe_2$.

In two previous papers (Bennema, Kremers, Meekes, Balzuweit & Verheijen, 1993; Kremers, Meekes, Bennema, Balzuweit & Verheijen, 1994), we have already outlined a superspace description for the morphology of an incommensurately modulated one-dimensional model crystal. Here, we first want to recall the ideas that have been used in this superspace description. One adopts the view that the presence of a flat face on the equilibrium morphology of a crystal is determined by the surface free energy of that face, because the crystal will take such a shape in equilibrium that the integrated surface free energy is minimal. Surface free energies are calculated by extending a broken-bond model to the embedding of the incommensurately modulated one-dimensional crystal in a $(1 + 1)$-dimensional superspace. Thus, a uniform bond density is obtained in this superspace. In addition, several crystallographic concepts are generalized. In this way, it is possible to show, in superspace, that the presence of an incommensurate modulation leads to a principle of selective cuts for the broken bonds. This principle implies that the average length of bonds intersected by a (satellite) face can be larger than the length that these bonds would have if there were no modulation. If a larger bond length corresponds to a lower bond energy, satellite faces (but also main faces) can be stabilized considerably and can appear on the equilibrium morphology of the crystal.

In the present paper, we treat equilibrium morphologies of incommensurately modulated three-dimensional crystals. They are embedded in a $(3 + 1)$-dimensional superspace. In essence, the situation comes down to the same $(1 + 1)$-dimensional analysis as treated by Kremers *et al.* (1994). It is shown that (satellite) faces on the physical crystal correspond to crystallographic hyperplanes of the embedded crystal. An important result of this paper is that this correspondence is one-to-one for the average energy of the (embedded) bonds broken by these planes. Consequently, it is in principle possible to

calculate the equilibrium morphology of any incommensurately modulated crystal using a superspace approach. Also, van Smaalen (1993) has reported a theory for the explanation of the stability of satellite faces. This author was able to derive an expression for the surface free energy of faces without making use of the superspace. We have agreed with van Smaalen (1994) to compare the results of the two theories very carefully in the near future. The benefits of using a superspace approach have been discussed by Bennema, Kremers, Meekes & Verheijen (1994). Moreover, they become apparent in the present report.

This paper is organized in the following manner. In §2, the model is presented for the description of an incommensurately modulated three-dimensional crystal. In addition, several problems are outlined that arise if one wants to calculate the surface free energies of faces within such a description. In §3, the embedding of the crystal model in a $(3+1)$-dimensional superspace is described. It is also explained how (chains of) bonds, as well as crystallographic hyperplanes, must be treated in this superspace. In §4, we show that there exists a one-to-one correspondence between such crystallographic hyperplanes and faces on the physical crystal for the morphology. We advise readers that are not interested in the details of this analysis to skip §4 and to go directly to §5. There, it is shown how this one-to-one correspondence can be used for the calculation of surface free energies and for the understanding of the principle of selective cuts. In §6, model calculations are presented by means of which the influence of several structural aspects on the equilibrium morphology is investigated. The basic assumptions that are used in this paper are critically discussed in §7, where also the consequences of the results obtained for actually occurring incommensurately modulated crystals are evaluated. Finally, conclusions are presented in §8.

2. The incommensurately modulated crystal

2.1. *Structure*

An incommensurate three-dimensional displacively modulated crystal can be modelled in the following way. There are j kinds of point-like atoms in the three-dimensional physical space. The positions of the atoms of kind j are given by position vectors $\mathbf{r}(\mathbf{n}, j)$:

$$\mathbf{r}(\mathbf{n}, j) = \mathbf{n} + \mathbf{r}_j + \mathbf{f}_j u_j(\mathbf{q} \cdot [\mathbf{n} + \mathbf{r}_j] + \varphi_j), \qquad (1)$$

where the last term describes the effect of the modulation. $\mathbf{n} = n_1\mathbf{a}_1 + n_2\mathbf{a}_2 + n_3\mathbf{a}_3$ with n_1, n_2 and $n_3 \in \mathbb{Z}$ and $\{\mathbf{a}_1, \mathbf{a}_2, \mathbf{a}_3\}$ forming the basis of a translation lattice Λ. The corresponding lattice translational symmetry is broken due to the modulation. In the three-dimensional space of the crystal, we define spatial positions

$$\mathbf{x} = x_1\mathbf{a}_1 + x_2\mathbf{a}_2 + x_3\mathbf{a}_3$$

by means of a set of three fractional coordinates (x_1, x_2, x_3) on the basis of Λ. The vector $\mathbf{r}_j$ gives for each atom kind j a (different) shift with respect to the point $\mathbf{n}$.

The modulation is characterized by the modulation function u_j, the modulation amplitude vector $\mathbf{f}_j$ and the modulation wave vector $\mathbf{q}$. The modulation function u_j is periodic in its argument: $u_j(\varphi) = u_j(\varphi + 1)$. This argument contains a constant phase factor φ_j that determines the shift of the modulation wave with respect to the origin. In principle, this phase factor can even be different for the x_1, x_2 and x_3 components, but the theory that we present applies to any modulation function, provided that the spatial variation of the argument of the function u_j is determined by $\mathbf{q} \cdot [\mathbf{n} + \mathbf{r}_j]$. We consider only one modulation wave vector $\mathbf{q}$ that is the same for all atoms, because this is the situation encountered for the majority of incommensurately modulated crystals known. The modulation wave vector is defined on the basis $\{\mathbf{a}_1^*, \mathbf{a}_2^*, \mathbf{a}_3^*\}$ of the reciprocal lattice Λ^*,

$$\mathbf{q} = q_1\mathbf{a}_1^* + q_2\mathbf{a}_2^* + q_3\mathbf{a}_3^*, \quad q_1, q_2, q_3 \in \mathbb{R}. \qquad (2)$$

A modulated crystal is called incommensurate if at least one of the numbers q_1, q_2 or q_3 is irrational. In that case, $\mathbf{q}$ builds a $\mathbb{Z}$-module of rank four together with $\mathbf{a}_1^*$, $\mathbf{a}_2^*$ and $\mathbf{a}_3^*$. This $\mathbb{Z}$-module is used, for example, to describe the positions of spots in the X-ray diffraction patterns of incommensurately modulated crystals. It thus carries the Fourier transform of the structure. In (1), the phase $\varphi = \mathbf{q} \cdot [\mathbf{n} + \mathbf{r}_j] + \varphi_j$ is determined, for each atom, by the modulation wave vector $\mathbf{q}$. Owing to the incommensurability, $\varphi \pmod 1$ takes infinitely many different irrational values in the interval [0,1) for an infinite crystal. Therefore, there exist for each atom kind j infinitely many different displacements from the positions $\mathbf{n} + \mathbf{r}_j$. This breaks the lattice translational symmetry.

Besides positions of atoms, a model for the morphology of crystals should further include (chemical) bonds. These are defined as line elements connecting any two different atomic positions. The bond energy depends both on the length of the bond and on the kinds of atom that are connected by the bond. It will be clear that, since the atomic positions are incommensurately modulated, there can also be infinitely many different bond lengths and corresponding bond energies.

2.2. *Incommensurability of the modulation wave vector*

It is important to discriminate between two possible types of modulation wave vectors $\mathbf{q}$ as defined by (2) because each type leads to a different (equilibrium) morphology. The two types correspond to the two ways in which $\mathbf{q}$ can be incommensurate with respect to the reciprocal lattice Λ^*.

In the first case, $\mathbf{q}$ has the same direction as some reciprocal-lattice vector $\mathbf{H} \in \Lambda^*$. The ratio of their lengths $|\mathbf{q}|/|\mathbf{H}|$, however, is an irrational number. For

this, it is necessary that at least one of the numbers q_1, q_2 or q_3 is irrational and that the ratio of any two of these numbers is rational. The modulation wave vector $\mathbf{q} = q_1\mathbf{a}_1^*$, with $q_1 \notin \mathbb{Q}$, is an example. We refer to this case as a modulation wave vector with an incommensurate length.

Alternatively, there may be no $\mathbf{H} \in \Lambda^*$ that points in the same direction as $\mathbf{q}$. In order to have this, the ratio of at least two of the three numbers q_1, q_2 and q_3 must be irrational. Certainly, one of these two numbers is then irrational. An example is the modulation wave vector $\mathbf{q} = \cos\theta\mathbf{a}_1^* + \sin\theta\mathbf{a}_2^*|\mathbf{a}_1^*|/|\mathbf{a}_2^*|$ with $\tan\theta \notin \mathbb{Q}$ and $\mathbf{a}_1^* \cdot \mathbf{a}_2^* = 0$, which has the same length as $\mathbf{a}_1^*$. We refer to this case as a modulation wave vector with an incommensurate direction.

Another classification of modulation wave vectors $\mathbf{q}$ is possible. Consider, in reciprocal space, all points $\mathbf{H} + m\mathbf{q}$ and let m run over all integral numbers and $\mathbf{H}$ over the reciprocal lattice Λ^*. Three different situations can be encountered. First, the points $\mathbf{H} + m\mathbf{q}$ can become dense on lines. The wave vector $\mathbf{q}$ then has an incommensurate length. Secondly, they can become dense on planes and lastly the points $\mathbf{H} + m\mathbf{q}$ may become dense on the whole space. The modulation wave vector has an incommensurate direction in the latter two cases. It is not necessary to make a distinction between these cases for the analysis presented in this paper.

2.3. *The intersection of bonds by crystallographic planes*

It has been shown experimentally (Janner, Rasing, Bennema & van der Linden, 1980; Dam, Janner, Bennema, van der Linden & Rasing, 1983; Dam *et al.*, 1985; Janner & Dam, 1989; Bennema *et al.*, 1991) that the orientation of faces on incommensurately modulated crystals can be described very accurately with four integral indices h_1, h_2, h_3 and h_4. These indices define a vector $\mathbf{H}_{(h_1h_2h_3h_4)}$ perpendicular to the face.

$$\begin{aligned}\mathbf{H}_{(h_1h_2h_3h_4)} &= h_1\mathbf{a}_1^* + h_2\mathbf{a}_2^* + h_3\mathbf{a}_3^* + h_4\mathbf{q} \\ &= (h_1 + h_4q_1)\mathbf{a}_1^* + (h_2 + h_4q_2)\mathbf{a}_2^* \\ &\quad + (h_3 + h_4q_3)\mathbf{a}_3^*. \qquad (3)\end{aligned}$$

Faces $(h_1h_2h_3h_4)$ for which $h_4 = 0$ are main faces and those with $h_4 \neq 0$ are satellite faces. The existence of the latter necessitates the use of four indices instead of three. Although this gives a satisfying description of the orientation of the faces that can occur, it does not explain why such (satellite) faces are stable. This is the reason that we want to be able to find the equilibrium morphology by means of a Wulff plot (Herring, 1951, 1953), using calculated surface free energies $\Gamma_{(h_1h_2h_3h_4)}$.

In the model, the surface free energy $\Gamma_{(h_1h_2h_3h_4)}$ (at $T = 0$) is defined as the energy per unit area necessary to create the face $(h_1h_2h_3h_4)$ from an infinite crystal by cutting bonds. The energy necessary to cut one specific bond is exactly the bond energy. For incommensurately modulated crystals, the calculation of $\Gamma_{(h_1h_2h_3h_4)}$ is not straightforward, however, because of the presence of infinitely many different bonds.

Consider a crystallographic plane $(h_1h_2h_3h_4)$. It can be constructed by positioning a plane such that it cuts $1/(h_1 + h_4q_1)$ of the a_1 axis, $1/(h_2 + h_4q_2)$ of the a_2 axis and $1/(h_3 + h_4q_3)$ of the a_3 axis. If the plane is not perpendicular to the modulation wave vector $\mathbf{q}$, there can be no two-dimensional lattice translational periodicity on this plane. In non-modulated crystals, on the other hand, there exists for each plane $(h_1h_2h_3)$ a two-dimensional unit cell, called mesh area $M_{(h_1h_2h_3)}$. The whole plane can then be covered by periodically repeating this mesh area. Consequently, for the calculation of the surface free energy of non-modulated crystals, it is sufficient to consider precisely one mesh area. On the contrary, crystallographic planes $(h_1h_2h_3h_4)$ of incommensurately modulated crystals, not perpendicular to $\mathbf{q}$, have no such mesh area. In order to calculate a $\Gamma_{(h_1h_2h_3h_4)}$, one can only average over the infinite plane.

For the crystallographic planes that are perpendicular to $\mathbf{q}$, it is essential to distinguish between the two types of modulation wave vector discussed in §2.2. If the modulation wave vector has an incommensurate direction, the only planes perpendicular to $\mathbf{q}$ are $(000h_4)$. There is again no mesh area on these planes owing to the incommensurate direction of $\mathbf{q}$ and one has to consider the whole plane. For a modulation wave vector with an incommensurate length, there is no unique set of indices for the plane perpendicular to it. Suppose that q_1 is non-zero. Then all planes $(h_1, h_1(q_2/q_1), h_1(q_3/q_1), h_4)$ with $h_1(q_2/q_1)$ and $h_1(q_3/q_1) \in \mathbb{Z}$ are perpendicular to $\mathbf{q}$ for any h_4. Moreover, on these planes there does exist a two-dimensional unit cell.

However, the latter special situation also differs from the case of a non-modulated crystal, despite the existence of a mesh area. This difference becomes apparent when we want to divide the crystal into identical slices. A face $(h_1h_2h_3)$ on a non-modulated crystal is assumed (Bennema, 1993) to grow with layers of thickness $d_{(h_1h_2h_3)} = |\mathbf{d}_{(h_1h_2h_3)}|$, where

$$\mathbf{d}_{(h_1h_2h_3)} = \mathbf{H}_{(h_1h_2h_3)}/|\mathbf{H}_{(h_1h_2h_3)}|^2. \qquad (4)$$

Using this $d_{(h_1h_2h_3)}$ as interplanar distance, one can define a grid of net planes. All planes of the grid are then equivalent, having the same surface free energy unless the three indices h_1, h_2 and h_3 have a common divisor larger than 1. In the case of an incommensurately modulated crystal, an analogous construction gives a grid of net planes with interplanar distance $d_{(h_1h_2h_3h_4)} = |\mathbf{d}_{(h_1h_2h_3h_4)}|$, where

$$\mathbf{d}_{(h_1h_2h_3h_4)} = \mathbf{H}_{(h_1h_2h_3h_4)}/|\mathbf{H}_{(h_1h_2h_3h_4)}|^2, \qquad (5)$$

where $\mathbf{H}_{(h_1h_2h_3h_4)}$ is given by (3). For the special case of a

modulation wave vector with an incommensurate length, however, we have seen that no unique grid can be defined perpendicular to **q**. Furthermore, owing to the intrinsic lack of translational symmetry along **q**, it is *a priori* not clear whether for any one of these grids all its net planes have equal surface free energy. For all other crystallographic planes $(h_1h_2h_3h_4)$, non-perpendicular to **q**, a unique grid is defined by (5). It is, however, again unclear whether the individual members of the grid have equal surface free energy, unless the face $(h_1h_2h_3h_4)$ is parallel to **q**. Also, in the case that the modulation wave vector has an incommensurate direction, one does not know *a priori* whether net planes of a grid have equal surface free energy.

It will be clear that one is faced with many problems in understanding the stability of faces $(h_1h_2h_3h_4)$ using the description of the incommensurately modulated structure defined by (1). Fortunately, a more elegant description is possible by making use of a space that has a dimension higher than three, the so-called superspace.

3. Embedding in superspace

3.1. *Structure in superspace*

The incommensurate crystal defined by (1) can be embedded (Janner & Janssen, 1977; de Wolff *et al.*, 1981; Janner, Janssen & de Wolff, 1983) in a $(3+1)$-dimensional superspace. Perpendicular to the physical space of the crystal, which is called external space, one defines a so-called internal space. In our model, the internal space has dimension 1 because there is only one modulation wave vector. The atoms of (1) are represented in superspace by wavy lines $\mathbf{r}_s(\mathbf{n}, j, \tau)$ extended along the internal direction:

$$\mathbf{r}_s(\mathbf{n}, j, \tau) = (\mathbf{n} + \mathbf{r}_j + \mathbf{f}_j u_j(\mathbf{q}\cdot[\mathbf{n}+\mathbf{r}_j] + \varphi_j + \tau), \tau). \quad (6)$$

The first three components of the right-hand side of (6) are in the external space and the fourth, τ, runs in the internal space. The wavy lines obtained in this way intersect the physical space ($\tau = 0$) exactly at the points defined by (1).

The advantage of this embedding is that the obtained structure has lattice translational symmetry in the superspace. There is a lattice Λ_s with basis $\{\mathbf{a}_{1s}, \mathbf{a}_{2s}, \mathbf{a}_{3s}, \mathbf{a}_{4s}\}$, where

$$\begin{aligned} \mathbf{a}_{1s} &= (\mathbf{a}_1, -q_1\mathbf{e}), \\ \mathbf{a}_{2s} &= (\mathbf{a}_2, -q_2\mathbf{e}), \\ \mathbf{a}_{3s} &= (\mathbf{a}_3, -q_3\mathbf{e}), \\ \mathbf{a}_{4s} &= (0, \mathbf{e}). \end{aligned} \quad (7)$$

Again, the first three components are in the external space and the fourth is in the internal space. The reciprocal lattice Λ_s^* then has the basis $\{\mathbf{a}_{1s}^*, \mathbf{a}_{2s}^*, \mathbf{a}_{3s}^*, \mathbf{a}_{4s}^*\}$, where

$$\begin{aligned} \mathbf{a}_{1s}^* &= (\mathbf{a}_1^*, 0) \\ \mathbf{a}_{2s}^* &= (\mathbf{a}_2^*, 0) \\ \mathbf{a}_{3s}^* &= (\mathbf{a}_3^*, 0) \\ \mathbf{a}_{4s}^* &= (\mathbf{q}, \mathbf{e}^*). \end{aligned} \quad (8)$$

Furthermore, $\mathbf{a}_{is}\cdot\mathbf{a}_{js}^* = \delta_{ij}$ and $\mathbf{e}\cdot\mathbf{e}^* = 1$.

We denote spatial positions in superspace by a set of four fractional coordinates: $(x_{1s}, x_{2s}, x_{3s}, x_{4s})$. This set represents the position vector:

$$\mathbf{x}_s = x_{1s}\mathbf{a}_{1s} + x_{2s}\mathbf{a}_{2s} + x_{3s}\mathbf{a}_{3s} + x_{4s}\mathbf{a}_{4s}.$$

It follows from (7) that any point (x_1, x_2, x_3) with respect to the basis $\{\mathbf{a}_1, \mathbf{a}_2, \mathbf{a}_3\}$ in the physical space is equal to the point $(x_1, x_2, x_3, q_1x_1 + q_2x_2 + q_3x_3)$ with respect to the basis $\{\mathbf{a}_{1s}, \mathbf{a}_{2s}, \mathbf{a}_{3s}, \mathbf{a}_{4s}\}$ in superspace.

3.2. *Modulated bond chains in superspace*

Consider, in the structure defined by (1), two atoms of the same kind j that would be translationally equivalent if there were no modulation. In that case, they would be separated by a so-called bond-chain vector

$$\mathbf{b} = (b_1, b_2, b_3), \quad b_1, b_2, b_3 \in \mathbb{Z}. \quad (9)$$

In such a non-modulated crystal, we have a so-called periodic bond chain (p.b.c.) (Hartman & Perdok, 1955; Bennema & van der Eerden, 1987; Bennema, 1993) if it is possible to construct an uninterrupted path of (one or more) bonds that connects the two translationally equivalent atoms. If a modulation is present, however, the p.b.c. can be deformed because the atoms may be displaced. We assume that, despite the deformation, all constituent bonds of the p.b.c. still exist and that no extra bonds are formed. Only the bond energies have changed. In this paper, we actually consider these modulated p.b.c.'s. We refer to them as modulated bond chains (m.b.c.).

In Fig. 2, an example is given of the embedding of a m.b.c. in superspace. The figure represents a view on the plane $V_{\mathbf{b},s}$ that is defined by the vectors $\mathbf{a}_{4s}$ and $\mathbf{b}_s$, where $\mathbf{b}_s$ is a lattice vector of Λ_s. One can construct $\mathbf{b}_s$ from the bond-chain vector $\mathbf{b}$ [(9)] in the following way:

$$\mathbf{b}_s = (b_1, b_2, b_3, 0). \quad (10)$$

The two vectors $\mathbf{b}_s$ and $\mathbf{a}_{4s}$ are basis vectors of a two-dimensional lattice Λ_b that can be constructed on $V_{\mathbf{b},s}$. Therefore, it is possible to define positions in the plane $V_{\mathbf{b},s}$ by means of a set of two fractional coordinates, $(x_{b1}, x_{b2})_{V_{\mathbf{b},s}}$. Such a set represents the position vector:

$$\mathbf{x}_s = x_{b1}\mathbf{b}_s + x_{b2}\mathbf{a}_{4s}.$$

Each translation vector of Λ_b must have integral x_{b1} and x_{b2} in this notation.

The two kinds of wavy lines in Fig. 2 represent the embedding of two different atoms, 1 and 2. The corresponding modulation amplitude vectors $\mathbf{f}_1$ and $\mathbf{f}_2$ are taken to have arbitrary (different) components in the three-dimensional physical space. This is depicted schematically in Fig. 2. The full-line parts of the wavy lines suggest that the wavy line is in front of the plane $V_{\mathbf{b},s}$ and the dashed parts that it is behind the plane. In a four-dimensional space, it is of course not unambiguously defined whether a point is behind or in front of a two-dimensional plane. Therefore, the figure is only a schematic representation of the actual situation.

In the physical space, all atoms 1 are connected by first-nearest-neighbour bonds with two atoms 2. Thus, a modulated bond chain is obtained, which has also been drawn schematically in Fig. 2.

The only part of the physical space present in the plane $V_{\mathbf{b},s}$ is a one-dimensional subspace containing $\mathbf{b}$. It is denoted $M_{\mathbf{b}}$. The m.b.c. winds its way everywhere in the close neighbourhood of this subspace. While travelling in $M_{\mathbf{b}}$ and starting from the origin, one enters after each distance $|\mathbf{b}|$ some new unit cell of the lattice Λ_b on $V_{\mathbf{b},s}$. In Fig. 2, this is demonstrated by means of the vectors $\mathbf{b}_2$ and $\mathbf{b}_3$ *etc.*, all having length $|\mathbf{b}|$. It is possible to assign to each vector $\mathbf{b}_i$, $i = 1, 2, 3, \ldots$, a specific part of the m.b.c. One can take, for example, that part of the m.b.c. that projects on $\mathbf{b}_i$ using orthogonal projections in the physical space. Using this construction, one is assured that every point of the m.b.c. is uniquely assigned to some vector $\mathbf{b}_i$.

It is important to realize that both $\mathbf{a}_{4s}$ and $\mathbf{b}_s$ are elements of the translation group of the whole embedded structure. Therefore, each vector $\mathbf{b}_i$ and its corresponding part of the m.b.c. is translationally equivalent to a vector $\mathbf{b}'_i$ starting in the first unit cell of Λ_b, together with an equivalent m.b.c. part. The vectors $\mathbf{b}'_2$ and $\mathbf{b}'_3$ have been drawn in Fig. 2. Owing to the incommensurability, all vectors $\mathbf{b}'_i$ intersect the $\mathbf{a}_{4s}$ axis at a different height in the first unit cell of Λ_b. The corresponding m.b.c. parts, therefore, form a uniform bond density in superspace in the same way as derived for a one-dimensional incommensurately modulated crystal by Kremers *et al.* (1994). This construction can, therefore, be considered to be a $(1 + 1)$-dimensional embedding of a m.b.c. Since there is a lattice Λ_b on $V_{\mathbf{b},s}$, it is also possible to define $(1 + 1)$-dimensional hyperplanes $(h_1, h_2)_s$ using the reciprocal lattice Λ_b^*. It is shown later that this is very useful.

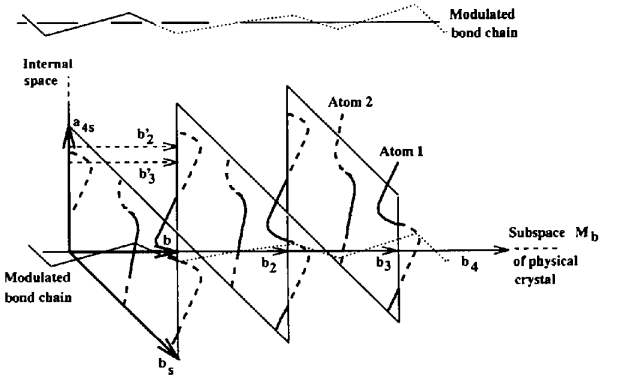

Fig. 2. The embedding in the plane $V_{\mathbf{b},s}$ of a modulated bond chain (m.b.c.) containing two kinds of atoms, 1 and 2. The m.b.c., which is entirely in the physical space, is represented by means of the physical subspace $M_{\mathbf{b}}$. Segments of the m.b.c. can be represented by vectors $\mathbf{b}_i$. For each vector $\mathbf{b}_i$, there exists a translationally equivalent vector $\mathbf{b}'_i$ in the first unit cell of the lattice Λ_b on $V_{\mathbf{b},s}$. In this way, a uniform bond density is constructed because the modulation is incommensurate. This is explained in the text.

3.3. *Crystallographic hyperplanes*

The embedded incommensurately modulated crystal, described in §3.1, has a lattice Λ_s. One can define crystallographic hyperplanes $(h_1h_2h_3h_4)_s$ as a straightforward extension of crystallographic planes in three dimensions by using the reciprocal lattice Λ_s^* (see Kremers *et al.*, 1994).

Thus, a crystallographic hyperplane $(h_1h_2h_3h_4)_s$ consists of all points $\mathbf{x}_s$ in superspace for which

$$\mathbf{H}_{(h_1h_2h_3h_4),s} \cdot \mathbf{x}_s = \text{constant}, \tag{11}$$

where $\mathbf{H}_{(h_1h_2h_3h_4),s}$ is defined as

$$\mathbf{H}_{(h_1h_2h_3h_4),s} = h_1\mathbf{a}^*_{1s} + h_2\mathbf{a}^*_{2s} + h_3\mathbf{a}^*_{3s} + h_4\mathbf{a}^*_{4s}. \tag{12}$$

The hyperplane $(h_1h_2h_3h_4)_s$ can be regarded as a plane of dimension 3 in the $(3 + 1)$-dimensional superspace, cutting the a_{1s} axis at $1/h_1$, the a_{2s} axis at $1/h_2$, the a_{3s} axis at $1/h_3$ and the a_{4s} axis at $1/h_4$ if the constant is 1. Owing to the $(3 + 1)$-dimensional lattice translational symmetry, one can define a mesh volume $M_{\mathbf{H},s}$ in the following way:

$$M_{\mathbf{H},s} = V_s/d_{\mathbf{H},s}, \tag{13}$$

where V_s is the volume of the unit cell of the lattice Λ_s and $d_{\mathbf{H},s}$ is the interplanar distance in a grid of identical net planes. This interplanar distance is defined as $d_{\mathbf{H},s} = |\mathbf{d}_{\mathbf{H},s}|$, where

$$\mathbf{d}_{\mathbf{H},s} = \mathbf{H}_{(h_1h_2h_3h_4),s}/|\mathbf{H}_{(h_1h_2h_3h_4),s}|^2. \tag{14}$$

The intersection of a crystallographic hyperplane $(h_1h_2h_3h_4)_s$ with the physical space is given by all points $\mathbf{x}_s$ that satisfy both (11) and $x_{4s} = q_1x_{1s} + q_2x_{2s} + q_3x_{3s}$. In this way, one derives that these are the points $\mathbf{x}$ in the physical space that satisfy

$$\begin{aligned}\mathbf{H}_{(h_1h_2h_3h_4)} \cdot \mathbf{x} &= x_1(h_1 + h_4q_1) + x_2(h_2 + h_4q_2) \\ &\quad + x_3(h_3 + h_4q_3) \\ &= \text{constant}.\end{aligned}$$

The intersection of a hyperplane $(h_1h_2h_3h_4)_s$ with the physical space is, therefore, exactly a (satellite) plane

$(h_1h_2h_3h_4)$. Furthermore, the grid of net planes $(h_1h_2h_3h_4)_s$, with interplanar distance $d_{\mathbf{H},s}$ in superspace, intersects the physical space exactly in the grid of net planes $(h_1h_2h_3h_4)$ with interplanar distance $d_{(h_1h_2h_3h_4)}$, given by (5).

Hence, it follows that (at least) all bonds cut by a single (satellite) plane $(h_1h_2h_3h_4)$ in the physical crystal are also cut by one hyperplane $(h_1h_2h_3h_4)_s$ in the embedded crystal in superspace. In the next section, we even show that, at least for planes $(h_1h_2h_3h_4)$ that are not perpendicular to the modulation wave vector $\mathbf{q}$, exactly the same bonds are cut by one mesh volume $M_{\mathbf{H},s}$ of the hyperplane $(h_1h_2h_3h_4)_s$ in superspace as by the (satellite) plane $(h_1h_2h_3h_4)$ in the physical crystal. This opens the way to the calculation of surface free energies $\Gamma_{(h_1h_2h_3h_4)}$ in superspace.

4. The one-to-one correspondence between crystallographic hyperplanes and (satellite) planes in the physical crystal

In this section, we show how to calculate the average energy of m.b.c. bonds, that are cut in the physical crystal by a certain plane $(h_1h_2h_3h_4)$. In order to obtain the surface free energy $\Gamma_{(h_1h_2h_3h_4)}$, this average energy must be multiplied for each kind of m.b.c. with the m.b.c. density, which is the number of that kind of m.b.c. that intersect the plane per unit area. The surface free energy $\Gamma_{(h_1h_2h_3h_4)}$ that we calculate is therefore the average energy per unit area that is necessary to create an infinitely large plane $(h_1h_2h_3h_4)$ by cutting bonds.

In order to find the average energy of all bonds cut by a certain plane $(h_1h_2h_3h_4)$ in the physical crystal, we use the fact that the physical space is a subspace of the superspace and that there is lattice translational symmetry in the latter. Each intersection point of the plane $(h_1h_2h_3h_4)$ with the m.b.c.'s of one kind in the physical space is in some unit cell of the lattice Λ_s. Owing to the lattice translational symmetry, there is in all cases an equivalent point in the first unit cell (containing the origin) of Λ_s. We consider the infinite set of points thus obtained in this first unit cell. The average energy that we seek is exactly the average energy of the bonds corresponding to the points in this set.

In addition, we calculate the intersection points of the corresponding $(h_1h_2h_3h_4)_s$ with the uniform bond density in superspace that corresponds to the chosen m.b.c. Again, all of these points are equivalent to points in the first unit cell of Λ_s. In this unit cell, we thus again obtain an infinite set of points. This set must contain the set of points that was constructed out of the intersection points in the physical crystal, because the physical crystal is contained in the embedded crystal and the m.b.c.'s are contained in the uniform bond density. For all planes, except a plane perpendicular to a $\mathbf{q}$ with an incommensurate length, it is hereafter shown that the two sets are identical. In these cases, there is a one-to-one correspondence between (satellite) planes and crystallographic hyperplanes as the calculation of surface free energies is concerned.

It is instructive to consider the following four cases:

(1) satellite faces non-perpendicular to the modulation wave vector;

(2) main faces non-perpendicular to the modulation wave vector;

(3) faces perpendicular to a modulation wave vector with an incommensurate direction;

(4) faces perpendicular to a modulation wave vector with an incommensurate length.

4.1. *Satellite faces non-perpendicular to the modulation wave vector*

Here, the situation is outlined for $(h_1h_2h_3h_4)$ planes, $h_4 \neq 0$, that are not perpendicular to $\mathbf{q}$. In this case, it is not necessary to discriminate between a $\mathbf{q}$ with an incommensurate direction and a $\mathbf{q}$ with an incommensurate length. The presented analysis applies for both types. This case can be considered as the generic case.

As described before, a m.b.c. is represented by means of the subspace $M_{\mathbf{b}}$ around which the m.b.c. winds its way. Although not essential, we assume for the ease of analysis that $M_{\mathbf{b}}$ contains the origin. To indicate this, it is denoted $M_{\mathbf{b}}(\mathbf{o})$. Because the incommensurately modulated crystal can be considered as a deformed three-dimensional basis structure that has a lattice Λ, all one-dimensional subspaces

$$M_{\mathbf{b}}(\mathbf{n}), \quad \mathbf{n} = (n_1, n_2, n_3) \in \Lambda, \tag{15}$$

represent a m.b.c. of the same kind. $M_{\mathbf{b}}(\mathbf{n})$ is the one-dimensional subspace obtained by translating all points of $M_{\mathbf{b}}(\mathbf{o})$ over the vector $\mathbf{n}$ in the physical space. The points $\mathbf{x}$ in these subspaces $M_{\mathbf{b}}(\mathbf{n})$ can be written as follows:

$$\mathbf{x} = x_{b1}\mathbf{b} + \mathbf{n}, \quad \forall x_{b1} \in \mathbb{R};\ n_1, n_2, n_3 \in \mathbb{Z}, \tag{16}$$

where $\mathbf{b}$ is given by (9). Transforming to the basis of the lattice Λ_s in superspace, these points become (see §3.1):

$$\mathbf{x}_s = (x_{b1}\mathbf{b} + \mathbf{n}, (x_{b1}\mathbf{b} + \mathbf{n}) \cdot \mathbf{q}). \tag{17}$$

It is important to keep in mind that all the points $\mathbf{x}_s \in M_{\mathbf{b}}(\mathbf{n})$ are in the physical space, although their coordinates are given with respect to Λ_s.

The uniform bond density that is obtained in superspace for these m.b.c.'s can accordingly be represented by planes

$$V_{\mathbf{b},s}(\mathbf{n}), \quad \mathbf{n} \in \Lambda \tag{18}$$

and the points on these planes can thus be written

$$\mathbf{x}_s = (x_{b1}\mathbf{b} + \mathbf{n}, x_{b2}), \quad \forall x_{b1}, x_{b2} \in \mathbb{R}. \tag{19}$$

In Fig. 3, an example is given of a crystal with only one kind of atom. Only a particular section (constant x_{3s}

coordinate) of the superspace has been drawn. M.b.c.'s are considered for which $\mathbf{b} = \mathbf{a}_1$ and $\mathbf{f} \parallel \mathbf{a}_1$. Three one-dimensional subspaces $M_{\mathbf{a}1}(\mathbf{o})$, $M_{\mathbf{a}1}(\mathbf{a}_2)$ and $M_{\mathbf{a}1}(2\mathbf{a}_2)$ have been drawn. The corresponding planes $V_{\mathbf{a}1,s}(\mathbf{o})$, $V_{\mathbf{a}1,s}(\mathbf{a}_2)$ and $V_{\mathbf{a}1,s}(2\mathbf{a}_2)$ have been indicated.

Consider now a crystallographic hyperplane $(h_1h_2h_3h_4)_s$. It has been shown in §3.3 that this hyperplane contains the satellite plane $(h_1h_2h_3h_4)$. This is demonstrated in Fig. 4 by drawing the $(11h_32)_s$ plane and the satellite plane $(11h_32)$ for the same situation as represented in Fig. 3. The intersections of the hyperplane with the subspaces $M_{\mathbf{b}}(\mathbf{n})$ represent, therefore, the intersection points of the (satellite) plane with the physical crystal. On the other hand, the intersections of the hyperplane with the planes $V_{\mathbf{b},s}(\mathbf{n})$ represent the intersection points of the hyperplane with the embedded structure in superspace, concerning the m.b.c. under study.

As described in §3.3, the crystallographic hyperplane $(h_1h_2h_3h_4)_s$ consists of all points $\mathbf{x}_s$ in superspace for which

$$\mathbf{H}_{(h_1h_2h_3h_4),s} \cdot \mathbf{x}_s = \text{constant}. \tag{20}$$

In Fig. 4, this constant is 2.

If we shift all points of the plane over a vector $\mathbf{d}_{\mathbf{H},s}$, we get a plane that is described by the following equation:

$$\mathbf{H}_{(h_1h_2h_3h_4),s} \cdot \mathbf{x}_s = \text{constant} + 1. \tag{21}$$

In the case that h_1, h_2, h_3 and h_4 have no common divisor larger than 1, this plane is translationally equivalent to the plane given by (20).

The intersection of the considered plane with the m.b.c.'s in the physical crystal is now obtained by substituting $\mathbf{x}_s \in M_{\mathbf{b}}(\mathbf{n})$ [(17)] for $\mathbf{x}_s$ in (20) and solving it for x_{b1}. The solution is

$$\begin{aligned} x_{b1} &= [\text{constant} - \mathbf{H}_{(h_1h_2h_3h_4),s} \cdot (\mathbf{n}, \mathbf{n} \cdot \mathbf{q})] \\ &\quad \times [\mathbf{H}_{(h_1h_2h_3h_4),s} \cdot (\mathbf{b}, \mathbf{b} \cdot \mathbf{q})]^{-1} \\ &= (\text{constant} - \mathbf{H}_{(h_1h_2h_3h_4)} \cdot \mathbf{n})/(\mathbf{H}_{(h_1h_2h_3h_4)} \cdot \mathbf{b}). \end{aligned} \tag{22}$$

For each subspace $M_{\mathbf{b}}(\mathbf{n})$, the required intersection point is determined by substituting this x_{b1} in (17). The intersection point is denoted $P_{\mathbf{b},\mathbf{H}}(\mathbf{n})$, but we immediately drop the $\mathbf{H}$ dependence in the notation and write $P_{\mathbf{b}}(\mathbf{n})$.

There is no solution in the case that the bond-chain vector $\mathbf{b}$ is parallel to the plane $(h_1h_2h_3h_4)$, which suggests that the plane does not cut any bonds. However, the atoms may be shifted out of the plane if their modulation amplitude vector has a component perpendicular to the plane. The bonds of the m.b.c. are then not necessarily parallel to the plane and can, therefore, be cut by the plane. Nevertheless, we do not take these m.b.c.'s into account because it is usually possible to shift the plane in the direction of its normal so that the bonds of the m.b.c. are no longer cut. This corresponds to a lower surface free energy and is, therefore, more favourable. We are interested, of course, in the lowest possible surface free energy.

Next, we calculate the intersection of the hyperplane $(h_1h_2h_3h_4)_s$ with the planes $V_{\mathbf{b},s}(\mathbf{n})$ by substituting $\mathbf{x}_s \in V_{\mathbf{b},s}$ [(19)] in (20). The solution is the line

$$\begin{aligned} x_{b1} &= [\text{constant} - \mathbf{H}_{(h_1h_2h_3h_4),s} \cdot (\mathbf{n}, x_{b2})] \\ &\quad \times [\mathbf{H}_{(h_1h_2h_3h_4),s} \cdot (\mathbf{b}, 0)]^{-1}. \end{aligned} \tag{23}$$

These lines should now be denoted $L_{\mathbf{b},\mathbf{H}}(\mathbf{n})$ but again we drop the $\mathbf{H}$ dependence. The lines $L_{\mathbf{b}}(\mathbf{n})$, of course, contain the points $P_{\mathbf{b}}(\mathbf{n})$. This is demonstrated in Fig. 5, again for the same situation as presented in Fig. 3.

Making use of the lattice translational symmetry in superspace one can translate the points $P_{\mathbf{b}}(\mathbf{n})$ and the lines $L_{\mathbf{b}}(\mathbf{n})$ to the $V_{\mathbf{b},s}(\mathbf{o})$ plane, by using the translation

$$\mathbf{n}_s = (-n_1, -n_2, -n_3, 0). \tag{24}$$

The obtained translationally equivalent points are

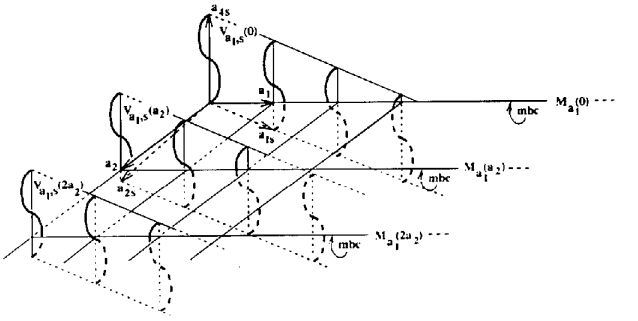

Fig. 3. A section at constant x_{3s} coordinate of the superspace embedding of an incommensurately modulated crystal. The vectors $\mathbf{a}_1$ and $\mathbf{a}_2$ define a plane in the physical crystal. The rest of the figure is outside the physical crystal. There is only one kind of atom, represented by the wavy lines; the solid parts are above the plane and the dashed parts are below. The modulation amplitude vector $\mathbf{f}$ is parallel to $\mathbf{a}_1$ and m.b.c.'s are considered for which $\mathbf{b} = \mathbf{a}_1$. Furthermore, $q_1 \neq 0$ and $q_2 \neq 0$ because $\mathbf{a}_{1s}$ differs from $\mathbf{a}_1$ and $\mathbf{a}_{2s}$ differs from $\mathbf{a}_2$. Three subspaces $M_{\mathbf{a}_1}(\mathbf{n})$, which all represent a m.b.c. of the same kind, have been drawn and the corresponding planes $V_{\mathbf{b}}(\mathbf{n})$ are indicated.

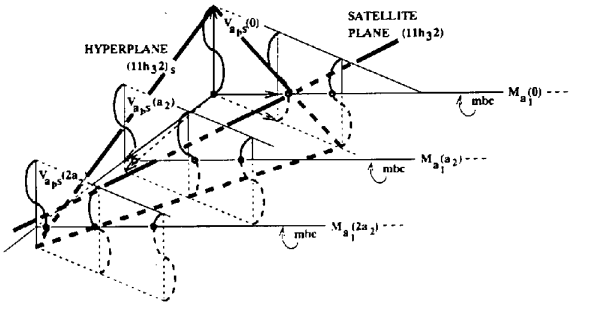

Fig. 4. The orientation of one hyperplane from the grid $(11h_32)_s$ in the same superspace embedding as used in Fig. 3. The hyperplane cuts the a_{1s} axis at 2, the a_{2s} axis at 2, the a_{3s} axis at $2/h_s$ and the a_{4s} axis at 1. The intersection of this hyperplane with the physical crystal is the satellite plane $(11h_32)$, which cuts the a_1 axis at $2/(1+2q_1)$, the a_2 axis at $2/(1+2q_2)$ and the a_3 axis at $2/(h_3+2q_3)$.

denoted $P'_{\mathbf{b}}(\mathbf{n})$ and the lines are denoted $L'_{\mathbf{b}}(\mathbf{n})$. In Fig. 6, these have been drawn for the example used in this section.

If we use the set of two coordinates with respect to the basis of the lattice Λ_b on $V_{\mathbf{b},s}(\mathbf{o})$, we obtain

$$P'_{\mathbf{b}}(\mathbf{n}) = (x_{b1}, x_{b1}(\mathbf{q}\cdot\mathbf{b}) + \mathbf{q}\cdot\mathbf{n})_{v_{\mathbf{b},s}(\mathbf{o})} \qquad (25)$$

with x_{b1} given by (22) and

$$L'_{\mathbf{b}}(\mathbf{n}) = (x_{b1}, x_{b2})_{v_{\mathbf{b},s}(\mathbf{o})}, \quad x_{b2} \in \mathbb{R} \qquad (26)$$

with x_{b1} given by (23).

The set of lines $L'_{\mathbf{b}}(\mathbf{n})$ in the plane $V_{\mathbf{b},s}(\mathbf{o})$ are equivalent to a grid of net planes $(h_1b_1 + h_2b_2 + h_3b_3, h_4)_s$ in the embedding of an incommensurately modulated one-dimensional crystal, with an average periodicity $a = |\mathbf{b}|$ and modulation

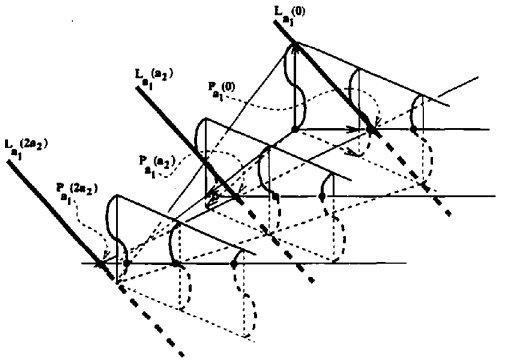

Fig. 5. The intersection of the hyperplane $(11h_32)_s$ (see Fig. 4) with the embedded m.b.c.'s (see Fig. 3) can be represented by lines $L_{\mathbf{a}_1}(\mathbf{n})$. These lines have the points $P_{\mathbf{a}_1}(\mathbf{n})$ in common with the physical crystal. The satellite plane $(11h_32)$ intersects the subspaces $M_{\mathbf{a}_1}(\mathbf{n})$ exactly at these points $P_{\mathbf{a}_1}(\mathbf{n})$.

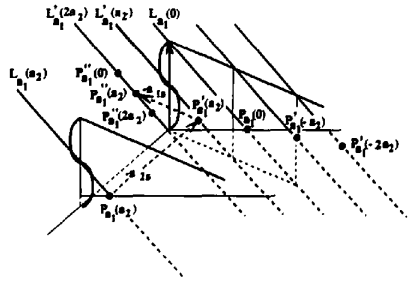

Fig. 6. From translation vectors of the lattice Λ_s, it is possible to find, in one $V_{\mathbf{b},s}$ plane, lines $L'_{\mathbf{a}_1}(\mathbf{n})$ equivalent to the lines $L_{\mathbf{a}_1}(\mathbf{n})$ that have been obtained in Fig. 5. As the intersection points $P_{\mathbf{a}_1}(\mathbf{n})$ can be found on the lines $L_{\mathbf{a}_1}(\mathbf{n})$, translationally equivalent points $P'_{\mathbf{a}_1}(\mathbf{n})$ can be found on the lines $L'_{\mathbf{a}_1}(\mathbf{n})$. In the plane $V_{\mathbf{b}_s}$, there is a lattice Λ_b. With translation vectors of this lattice, it is possible to show that all lines $L'_{\mathbf{a}_1}(\mathbf{n})$ are translationally equivalent. The line $L'_{\mathbf{a}_1}(\mathbf{a}_2)$, for example, is translationally equivalent (using the vector $\mathbf{a}_{1s}$) to the line $L'_{\mathbf{a}_1}(2\mathbf{a}_2)$. As the points $P'_{\mathbf{a}_1}(\mathbf{n})$ are on the lines $L'_{\mathbf{a}_1}(\mathbf{n})$, translationally equivalent points $P''_{\mathbf{a}_1}(\mathbf{n})$ can be found on the line $L'_{\mathbf{a}_1}(2\mathbf{a}_2)$. This line can be considered as a lattice plane defined on Λ_b in $V_{\mathbf{b},s}$. It can be shown that the points $P''_{\mathbf{a}_1}(\mathbf{n})$ become dense on a single mesh area of this $(1+1)$-dimensional lattice plane.

wave vector $q = (\mathbf{q}\cdot\mathbf{b})a^*$. We have shown in a previous paper (Kremers *et al.*, 1994) that in such a $(1+1)$-dimensional case all members of the grid of net planes $(h_1h_2)_s$ [here corresponding to the lines $L'_{\mathbf{b}}(\mathbf{n})$] are translationally equivalent and that all intersection points of the grid with the one-dimensional modulated crystal [here corresponding to the subspace $M_{\mathbf{b}}(\mathbf{o})$] become dense on a single mesh area $M_{(h_1h_2),s}$ of one member of the grid, if translations of the $(1+1)$-dimensional lattice are used. The only difference between that case and the present one is that the points $P'_{\mathbf{b}}(\mathbf{n})$ in which we are interested are not all in the one-dimensional physical subspace $M_{\mathbf{b}}(\mathbf{o})$ but instead only one point is. For the example, this can be seen in Fig. 6.

However, for the same reasons as described by Kremers *et al.* (1994), all lines $L'_{\mathbf{b}}(\mathbf{n})$ are translationally equivalent (unless $h_1b_1 + h_2b_2 + h_3b_3$ and h_4 have a common divisor larger than 1). Consequently, we arrive at the important conclusion that the intersection of a hyperplane $(h_1h_2h_3h_4)_s$ with the uniform bond density corresponding to a m.b.c. with bond-chain vector $\mathbf{b}$ can be found by considering one mesh area of one line $L'_{\mathbf{b}}(\mathbf{n})$ in a $(1+1)$-dimensional description of the m.b.c.

Subsequently, we want to show that also all points $P'_{\mathbf{b}}(\mathbf{n})$ become dense on one such mesh area of a line $L'_{\mathbf{b}}(\mathbf{n})$. This can be made clear in the following way. Since the lines $L'_{\mathbf{b}}(\mathbf{n})$ behave as a grid of net planes on the lattice Λ_b of $V_{\mathbf{b},s}(\mathbf{o})$, one can find, for each single line, a translation

$$\mathbf{n}_v = (n_{b1}, n_{b2})_{v_{\mathbf{b},s}(\mathbf{o})}, \quad n_{b1}, n_{b2} \in \mathbb{Z} \qquad (27)$$

such that the line is translated onto one specific line $L'_{\mathbf{b}}$. Thus, we obtain points $P''_{\mathbf{b}}(\mathbf{n})$ (see Fig. 6) that are on the chosen line $L'_{\mathbf{b}}$, having a coordinate $x_{b1} - n_{b1}$ with $n_{b1} \in \mathbb{Z}$ and x_{b1} given by (22). Owing to the incommensurability, x_{b1} is always an irrational number and, therefore, also $x_{b1} - n_{b1}$ is irrational. On the line $L'_{\mathbf{b}}$ there is a periodicity of h_4 in the x_{b1} coordinate because the slope is equal to $-(h_1b_1 + h_2b_2 + h_3b_3)/h_4$. Owing to this periodicity and the irrationality of $x_{b1} - n_{b1}$, the points $P''_{\mathbf{b}}(\mathbf{n})$ become dense on the line $L'_{\mathbf{b}}$. This can be proven by following the same arguments as used in the proof of the existence of a uniform bond density in the $(1+1)$-dimensional superspace of an incommensurately modulated one-dimensional crystal, as has been given by Kremers *et al.* (1994).

Thus, we have shown that the intersection of a (satellite) plane with a m.b.c. of the physical crystal, having bond-chain vector $\mathbf{b}$, can also be found by considering one mesh area of one single line $L'_{\mathbf{b}}(\mathbf{n})$ in a $(1+1)$-dimensional embedding of the m.b.c. This opens the way for inspecting the bonds that are cut by the satellite plane by means of a graphical method. For each m.b.c., one draws the corresponding $(1+1)$-dimensional embedding of the m.b.c. The intersection points can then be found by drawing the $(1+1)$-dimensional plane $(h_1b_1 + h_2b_2 + h_3b_3, h_4)_s$.

When $h_1b_1 + h_2b_2 + h_3b_3$ and h_4 have some common divisor $d \in \mathbb{Z}$, not all lines $L'_{\mathbf{b}}(\mathbf{n})$ are translationally equivalent but there are d different non-translationally equivalent lines. However, for each of these lines, there are still infinitely many translationally equivalent lines $L'_{\mathbf{b}}(\mathbf{n})$. The points $P''_{\mathbf{b}}(\mathbf{n})$ on one such subset of all lines $L'_{\mathbf{b}}(\mathbf{n})$ become dense on a single line of the subset. This holds for all d different non-translationally equivalent lines.

It is concluded that for planes $(h_1h_2h_3h_4)$ non-perpendicular to $\mathbf{q}$ there exists a one-to-one correspondence between the intersection of the hyperplane $(h_1h_2h_3h_4)_s$ with the embedded structure and the intersection of the (satellite) plane with the physical crystal. Furthermore, this conclusion can be drawn for each value of the constant in (20). This implies that there is also a one-to-one correspondence between the satellite planes corresponding to two hyperplanes $(h_1h_2h_3h_4)_s$ that are an integer number times $\mathbf{d}_{\mathbf{H},s}$ apart because these hyperplanes are translationally equivalent. Therefore, the average energy of the bonds cut by a plane $(h_1h_2h_3h_4)$ in the physical crystal is equal to that of the bonds cut by a plane with the same orientation but shifted over a vector $\mathbf{d}_{(h_1h_2h_3h_4)}$ with respect to the original plane. Consequently, the physical crystal can be partitioned in slices with thickness $|\mathbf{d}_{(h_1h_2h_3h_4)}|$ that all have exactly the same energy content $E_{\mathbf{H}}$. The difference between this $E_{\mathbf{H}}$ and the classical notion E_{slice} is addressed in the *Discussion*. The remaining question is whether the surface free energy depends on the exact position of the surface of the slice. This position is determined by the value of the constant in (20).

In this section, it has been shown that, in order to find the average energy of the bonds that are cut in the physical crystal by a plane $(h_1h_2h_3h_4)$, it is sufficient to average over the energy of the embedded bonds that are cut in superspace by a hyperplane $(h_1h_2h_3h_4)_s$. However, the latter is equal to averaging over one mesh volume $M_{\mathbf{H},s}$ of the hyperplane because the embedded structure has a lattice. This, in turn, is equal to averaging over all embedded bonds that are cut in one unit cell of Λ_s by the grid of net planes $(h_1h_2h_3h_4)_s$ (Heijmen, Kremers & Meekes, 1994).

4.2. *Main faces non-perpendicular to the modulation wave vector*

Main faces, on the incommensurately modulated crystals that we consider, are $(h_1h_2h_30)$ planes. Here, we consider only those $h_4 = 0$ planes that are not perpendicular to the modulation wave vector $\mathbf{q}$. In the case that $\mathbf{q}$ has an incommensurate direction, there is even no main face perpendicular to it. Although $(h_1h_2h_30)$ planes have the same orientation as $(h_1h_2h_3)$ planes would have if the modulation were absent, their surface free energy can definitely be changed by the modulation. Using the generic case that has been described in §4.1, one can derive that there is again a one-to-one correspondence between a main face $(h_1h_2h_30)$ and the crystallographic hyperplane $(h_1h_2h_30)_s$.

Such a hyperplane has a special orientation in superspace in the sense that it is parallel to the internal space. This means that all lines $L_{\mathbf{b}}$, obtained by intersecting the hyperplane with an embedded m.b.c., are also parallel to the internal space. Following the same procedure as described in §4.1, one finds lines

$$L'_{\mathbf{b}}(\mathbf{n}) = (x_{b1}, x_{b2})_{v_{\mathbf{b},s}(\mathbf{o})}, \quad x_{b2} \in \mathbb{R},$$

where

$$x_{b1} = (\text{constant} - \mathbf{H}_{(h_1h_2h_30)} \cdot \mathbf{n})/(\mathbf{H}_{(h_1h_2h_30)} \cdot \mathbf{b})$$

is independent of x_{b2}. These lines $L'_{\mathbf{b}}(\mathbf{n})$ can be translated onto $|h_1b_1 + h_2b_2 + h_3b_3|$ lines $L'_{\mathbf{b}}$ through the first unit cell of the lattice Λ_b. The points $P''_{\mathbf{b}}(\mathbf{n})$ on these lines that are translationally equivalent to the intersection points of the main face $(h_1h_2h_30)$ with the physical crystal, then have x_{b2} coordinate

$$x_{b2} = \{[(\mathbf{q} \cdot \mathbf{b})(\text{constant} - \mathbf{H}_{(h_1h_2h_30)} \cdot \mathbf{n})] \times (\mathbf{H}_{(h_1h_2h_30)} \cdot \mathbf{b})^{-1}\} + (\mathbf{q} \cdot \mathbf{n}).$$

Since there is a translational periodicity of 1 on the x_{b2} coordinate, the points $P''_{\mathbf{b}}(\mathbf{n})$ become dense on the $|h_1b_1 + h_2b_2 + h_3b_3|$ lines. Therefore, the same bonds are cut in the intersection of a main face $(h_1h_2h_30)$ with the physical crystal as in the intersection of one mesh volume $M_{\mathbf{H},s}$ of the hyperplane $(h_1h_2h_30)_s$ with the embedded m.b.c. This can be inspected graphically by drawing $(1+1)$-dimensional $(h_1b_1 + h_2b_2 + h_3b_3, 0)_s$ planes in the corresponding $(1+1)$-dimensional embeddings of the m.b.c.'s present in the crystal.

Furthermore, for the same reasons as given in §4.1, the crystal can be partitioned in $(h_1h_2h_30)$ slices with thickness $|\mathbf{d}_{(h_1h_2h_30)}|$ that all have exactly the same energy content and surface free energy. The latter, however, may depend on the exact position of the surface.

4.3. *Faces perpendicular to a modulation wave vector with an incommensurate direction*

The only faces perpendicular to a modulation wave vector $\mathbf{q}$ with an incommensurate direction are $(000h_4)$ planes. Also for these planes one can follow the lines of thought as used in the generic case that has been described in §4.1. The lines $L'_{\mathbf{b}}(\mathbf{n})$ are then found to be

$$L'_{\mathbf{b}}(\mathbf{n}) = (x_{b1}, \text{constant}/h_4)_{v_{\mathbf{b},s}(\mathbf{o})}, \quad x_{b1} \in \mathbb{R}.$$

Therefore, they are all equal and parallel to the b_s axis. The points $P''_{\mathbf{b}}(\mathbf{n})$, corresponding to the intersection points in the physical crystal have x_{b1} coordinates

$$x_{b1} = [\text{constant} - h_4(\mathbf{q} \cdot \mathbf{n})]/h_4(\mathbf{q} \cdot \mathbf{b})$$

on this line.

If we choose $h_4 = 1$, the intersection points in the physical crystal can be inspected graphically by drawing $(01)_s$ planes in the $(1 + 1)$-dimensional embeddings of the m.b.c.'s present in the crystal.

In this case, the crystal can be partitioned in (0001) slices with thickness $|\mathbf{d}_{(0001)}|$ that all have the same energy content and the same surface free energy. Again, it is expected that this surface free energy depends on the exact position of the surface.

4.4. *Faces perpendicular to a modulation wave vector with an incommensurate length*

When one is dealing with a modulation wave vector $\mathbf{q}$, having an incommensurate length, there is a special plane that requires a treatment clearly different from the analysis outlined in §4.1 (see also van Smaalen, 1993). This is the plane that is perpendicular to $\mathbf{q}$. It has been explained in §2.3 that on such a plane there does exist a two-dimensional unit cell, contrary to the cases that have been treated in §§4.1, 4.2 and 4.3. Therefore, there can only be a finite number of different bonds that are cut by that plane.

In view of §§4.2 and 4.3, it is interesting to realize that the plane can be considered to be a main plane $(h_1, h_1(q_2/q_1), h_1(q_3/q_1), 0)$ with $h_1(q_2/q_1)$ and $h_1(q_3/q_1) \in \mathbb{Z}$ as well as a $(000h_4)$ satellite plane. (We have conveniently taken $q_1 \neq 0$.) This implies that the plane perpendicular to $\mathbf{q}$ is contained in the hyperplane $(h_1, h_1(q_2/q_1), h_1(q_3/q_1), 0)_s$ as well as in the hyperplane $(000h_4)_s$. It is, therefore, (contained in) the intersection of these two hyperplanes. We want to point out that an analogous situation is encountered for quasiperiodic tilings (Heijmen, Kremers, Meekes & Janssen, 1995). For such tilings, however, the situation is generic, whereas it is a special case for an incommensurately modulated crystal.

Although we are dealing with a special situation, it is still possible to use the superspace embedding of the structure in order to find the intersection points of the plane perpendicular to $\mathbf{q}$ with the physical crystal. Consider the hyperplane $(h_1, h_1(q_2/q_1), h_1(q_3/q_1), 0)_s$. Its intersections with the subspaces $M_\mathbf{b}(\mathbf{n})$ that represent the m.b.c.'s can be calculated in the same way as described in §4.1. The intersection points $P_\mathbf{b}(\mathbf{n})$ are given by putting x_{b1} in (17) equal to

$$x_{b1} = [\text{constant} - (h_1/q_1)(\mathbf{q} \cdot \mathbf{n})] \times [h_1 b_1 + h_1(q_2/q_1)b_2 + h_1(q_3/q_1)b_3]^{-1}. \quad (28)$$

One then finds the following condition for the x_{b2} coordinate:

$$x_{b2} = (q_1/h_1)\ \text{constant}. \quad (29)$$

This condition, however, exactly expresses that all intersection points $P_\mathbf{b}(\mathbf{n})$ are on a crystallographic hyperplane $(000h_4)_s$. The points $P_\mathbf{b}(\mathbf{n})$ can again be translated to the $V_{\mathbf{b},s}(\mathbf{o})$ plane with lattice vectors of the lattice Λ_s so that equivalent points $P'_\mathbf{b}(\mathbf{n})$ are obtained. With the set of two coordinates $(x_{b1}, x_{b2})_{V_{\mathbf{b},s}(\mathbf{o})}$ defined with respect to the basis of the lattice Λ_b on this plane, the points $P'_\mathbf{b}(\mathbf{n})$ can be written

$$P'_\mathbf{b}(\mathbf{n}) = (x_{b1}, (q_1/h_1)\ \text{constant})_{V_{\mathbf{b},s}(\mathbf{o})},$$

where x_{b1} is given by (28). All the points $P'_\mathbf{b}(\mathbf{n})$ lie on the lines $L'_\mathbf{b}(\mathbf{n})$ that would have been found if the intersection lines $L_\mathbf{b}(\mathbf{n})$ of the embedded m.b.c. with the hyperplane $(h_1, h_1(q_2/q_1), h_1(q_3/q_1), 0)_s$ would have been translated to the $V_{\mathbf{b},s}(\mathbf{o})$ plane. Therefore, it is tempting to look at the situation again as a grid of $(h_1 b_1 + h_2 b_2 + h_3 b_3, 0)_s$ planes in the $(1 + 1)$-dimensional embedding of the m.b.c. However, this case differs from the situation described in §4.2, as the points now all have equal x_{b2} coordinate. Therefore, if one tries to translate these point to points $P''_\mathbf{b}(\mathbf{n})$ in the first unit cell of the lattice Λ_b only $|h_1 b_1 + h_2 b_2 + h_3 b_3|$ different points $P''_\mathbf{b}(\mathbf{n})$ are obtained, instead of infinitely many. This may be expected because a two-dimensional unit cell can be defined on the plane and, as we show in §6, the m.b.c. density is indeed $|h_1 b_1 + h_2 b_2 + h_3 b_3|$ divided by the area of that two-dimensional unit cell.

The intersection points with the physical crystal of a plane perpendicular to a $\mathbf{q}$ that has an incommensurate length can thus be found by considering the intersection points of a grid of $(h_1 b_1 + h_2 b_2 + h_3 b_3, 0)_s$ planes with a $(0, 1)_s$ hyperplane in a $(1 + 1)$-dimensional embedding of a m.b.c. This situation is clearly exceptional because it is the only one in which there is no one-to-one correspondence between the plane in the physical crystal and the corresponding hyperplane.

Furthermore, one can in this case not derive that it is possible to partition the crystal in $(h_1, h_1(q_2/q_1), h_1(q_3/q_1), 0)$ slices with the same energy content or with the same surface free energy. That is, if we consider a plane $(h_1, h_1(q_2/q_1), h_1(q_3/q_1), 0)$ that has been shifted over a vector $\mathbf{d}_{(h_1, h_1(q_2/q_1), h_1(q_3/q_1), 0)}$ with respect to the plane just described, similar results to (28) and (29) are found, the only difference being that the value of the constant has increased with 1. This means that the points $P'_\mathbf{b}(\mathbf{n})$ are again on the grid of $(h_1 b_1 + h_2 b_2 + h_3 b_3, 0)_s$ planes but have a different x_{b2} coordinate:

$$x_{b2} = (q_1/h_1)\ \text{constant} + q_1/h_1.$$

One thus obtains a different set of $|h_1 b_1 + h_2 b_2 + h_3 b_3|$ points, which means that the average energy of the bonds that are cut by the plane is, in principle, also different. Shifting the plane any integer, $p \in \mathbb{Z}$, times $\mathbf{d}_{(h_1, h_1(q_2/q_1), h_1(q_3/q_1), 0)}$ never gives an equivalent set of intersection points because in all these cases an irrational number $p(q_1/h_1)$ is added to the x_{b2} coordinate of the points $P'_\mathbf{b}(\mathbf{n})$ and there is a translational periodicity of one in the x_{b2} coordinate.

In order to study the average energy of the bonds that are cut as a function of position of the plane, one must vary the position of the grid $(h_1b_1 + h_2b_2 + h_3b_3, 0)_s$ as well as the position of the $(0, 1)_s$ hyperplane. Each set of intersection points that is obtained in this way corresponds to some position of the plane perpendicular to $\mathbf{q}$ in the physical crystal.

Thus, this case is indeed exceptional.

5. Principle of selective cuts

In this section, we demonstrate the principle of selective cuts. It has been shown by Kremers *et al.* (1994) how, for an incommensurately modulated one-dimensional crystal, this principle is the cause of the stabilization of (satellite) faces, *i.e.* the lowering of surface free energy. Also, for incommensurately modulated three-dimensional crystals, there is a lowering of the surface free energy caused by the principle of selective cuts.

In §4, it has been shown that the average energy of the bonds that are cut in the physical crystal by a certain $(h_1h_2h_3h_4)$ plane can be found, in general, in superspace by averaging over all embedded bonds that are cut by one mesh volume of the corresponding hyperplane $(h_1h_2h_3h_4)_s$. Although the approach of §4 is not valid for commensurately modulated crystals ($q_1, q_2, q_3 \in \mathbb{Q}$), it can be applied to incommensurately modulated crystals for which the modulation amplitude vector $\mathbf{f}$ has zero length. In that case, however, the structure does not differ from the non-modulated crystal. The wavy lines in superspace that represent the atoms become straight lines and the modulated bond chains are no longer modulated. For convenience, let us consider m.b.c.'s that consist of one type of atom and one type of bond. In the embedding of this m.b.c., only one bond length is found in the uniform bond density in superspace. Consequently, the average length of the embedded bonds that are cut by the mesh volume of any hyperplane is a constant, *i.e.* equal to the length of the non-modulated bond. This implies that, for a crystal that is not modulated, it is the number of intersected bonds per unit area, which is the so-called m.b.c. density, that determines the surface free energy. It is well known, however, that in that case cusps appear in a polar plot of the surface free energy only for (*hkl*) planes, *i.e.* a Wulff plot (Bennema & van der Eerden, 1987). Only these planes, therefore, can appear in the equilibrium form of a non-modulated crystal.

Let us now consider an incommensurately modulated crystal with a non-zero modulation amplitude. Although the atoms are displaced due to the modulation, we have assumed that with respect to p.b.c.'s for the non-modulated case no bonds disappear and no extra bonds appear in m.b.c.'s of the modulated crystal. This means that for an infinite plane the average number of intersected m.b.c.'s per unit area is the same as the number intersected in the non-modulated case, unless the modulation amplitude is very large. Since we calculate surface free energies as average broken-bond energies over infinite planes, it cannot be this m.b.c. density that changes the surface free energy for an incommensurately modulated crystal. Therefore, if the surface free energy of satellite faces can be lowered due to the modulation so that they have a chance of appearing on the equilibrium form, this must be caused by the fact that the average broken-bond energy can be lower than the energy of a non-modulated bond. In general, this is possible because a mesh volume of a hyperplane can intersect only a selection of all possible bonds that can be found in superspace. We reach the conclusion that the stabilization of (satellite) planes is caused by a principle of selective cuts. This principle is now demonstrated for the four cases described in §4. We treat them in the order of increasing possible stabilization of surface free energy.

5.1. *Main faces non-perpendicular to the modulation wave vector*

It has been shown in §4.2 that for main faces one must inspect the embedded bonds that are cut by a grid of $(h_1b_1 + h_2b_2 + h_3b_3, 0)_s$ planes in the $(1 + 1)$-dimensional embedding of a m.b.c. As an example, we take $\mathbf{b} = \mathbf{a}_1$ and $\mathbf{f} \| \mathbf{a}_1$ and consider the (1110) plane so that the grid is $(1, 0)_s$. From the analysis in §4.2, we have also learned that the surface free energy is expected to depend on the position of the plane, with a periodicity of $|\mathbf{d}_{(h_1h_2h_30)}|$.

In Fig. 7, the situation is presented for two (1110) planes at different positions and the bonds that are cut by one mesh area have been indicated. For the first position, all possible different bonds are cut so that the average energy is equal to the energy of a non-modulated bond. The second position, however, demonstrates that it is possible to position the plane such that relatively more

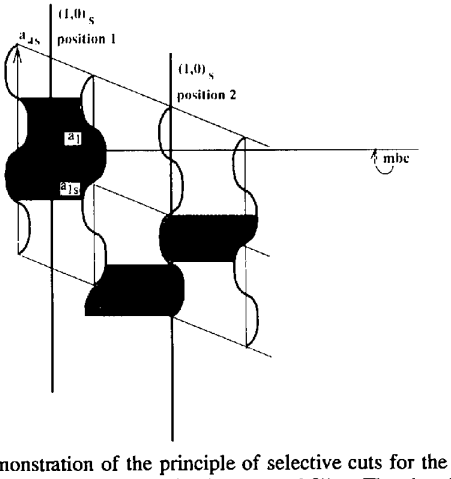

Fig. 7. Demonstration of the principle of selective cuts for the (1110) plane cutting m.b.c.'s for which $\mathbf{b} = \mathbf{a}_1$ and $\mathbf{f} \| \mathbf{a}_1$. The situation can be represented with a $(1, 0)_s$ plane intersecting the bonds in a $(1 + 1)$-dimensional embedding of the m.b.c. The cut bonds have been shaded. Two different positions for the plane represent the variation of surface free energy within a distance $d_{(1110)}$.

long than short bonds are cut. This is an example of the principle of selective cuts. The average energy will be lower than the energy of the non-modulated bond. Main faces non-perpendicular to the modulation wave vector can thus have a lower surface free energy than they would have in the non-modulated case.

The amount of stabilization for a certain plane depends, of course, on the shape of the modulation function u, the magnitude and direction of the modulation amplitude vector $\mathbf{f}$ and the magnitude and direction of the modulation wave vector $\mathbf{q}$. It is not straightforward to predict the dependence on u. The dependence on $\mathbf{f}$ is, however, clear. The larger the amplitude $|\mathbf{f}|$ and the larger the value of $|\mathbf{f} \cdot \mathbf{b}|$, the larger the amount of stabilization. In both cases, a larger value implies that larger bond lengths can be found in the crystal.

For the influence of the direction of the modulation wave vector, one must again discriminate between a modulation wave vector with an incommensurate length and with an incommensurate direction. In the case of an incommensurate length, there can be m.b.c.'s for which $\mathbf{b} \perp \mathbf{q}$. These must then be periodic bond chains. They can differ from what they would be in the case that the modulation was absent, if they are built out of more than one kind of bond. Nevertheless, these m.b.c.'s contain only a finite number of different bonds, so that in their embedding also only a finite number of different bond lengths appear. This implies that there can be no selective cutting. In the case of a modulation wave vector with an incommensurate direction, all m.b.c.'s are indeed modulated, so that every m.b.c. contains an infinite number of different bonds. Furthermore, the distinction between the two types of modulation wave vector is essential for the amount of stabilization of planes perpendicular to $\mathbf{q}$. This, however, is explicitly treated below.

Also, the length of the modulation wave vector influences the amount of stabilization. As explained in §4.1, one can consider the $(1+1)$-dimensional embedding of the m.b.c. to have a modulation wave vector $q = (\mathbf{q} \cdot \mathbf{b})a^*$. The dependence on the length of such a vector q has already been outlined by Kremers *et al.* (1994) for a longitudinal modulation, $\mathbf{f} \| \mathbf{b}$. In that paper, we studied the dependence on the value of q_1 for an incommensurately modulated one-dimensional crystal and we refer to Fig. 5 of this reference. This figure can still be used for the overall behaviour in the case that the modulation is not longitudinal.

5.2. *Satellite faces non-perpendicular to the modulation wave vector*

The case of satellite faces $(h_1h_2h_3h_4)$, $h_4 \neq 0$, has been treated in §4.1. In Fig. 8, the $(1, 2)_s$ plane has been drawn representing the (1112) plane and the $(0, 1)_s$ plane representing the (0111) plane. Here, $\mathbf{b} = \mathbf{a}_1$ and $\mathbf{f} \| \mathbf{a}_1$ also. The positions of the planes can again be varied over distances $|\mathbf{d}_{(1112)}|$ and $|\mathbf{d}_{(0111)}|$, respectively, in order to study the dependence of the surface free energy on the position. For the (1112) plane, this is equal to varying the position at which the hyperplane cuts the a_{4s} axis between $0\mathbf{a}_{4s}$ and $\frac{1}{2}\mathbf{a}_{4s}$. For the (0111) plane, the intersection point at the a_{4s} axis must be varied between $0\mathbf{a}_{4s}$ and $1\mathbf{a}_{4s}$.

Fig. 8 clearly shows that the $(0, 1)_s$ plane cuts only a small fraction of all possible bonds, whereas the $(1, 2)_s$ plane cuts all possible different bonds at least once, and a large fraction of them even twice. It is important to realize that the $(01)_s$ plane is so selective in Fig. 8 because the value of q_1 in this $(1+1)$-dimensional embedding is about 0.26. The largest stabilization of the $(01)_s$ plane can be reached for $q_1 = 0.35$ (see Kremers *et al.*, 1994). In the case when q_1 is close to 0.65, one would expect $(1\bar{1})$ to be highly selective.

The amount of stabilization with respect to the non-modulated crystal again depends on the modulation function u, the modulation amplitude vector $\mathbf{f}$ and the modulation wave vector $\mathbf{q}$ in the same way as described in §5.1. Furthermore, Fig. 8 shows that, in general, there can be more stabilization when the mesh area of the $(h_1b_1 + h_2b_2 + h_3b_3, h_4)_s$ plane is smaller. In order to have such a small mesh area, both $h_1b_1 + h_2b_2 + h_3b_3$ and h_4 must be small. Therefore, as a rule of thumb, one can state that the smaller the indices h_1, h_2, h_3 and h_4 the larger the stabilization. The same rule of thumb is often used for $(h_1h_2h_3)$ planes in non-modulated crystals.

In general, one can expect that there exists a selected number of satellite faces that have a relatively larger stabilization than the main faces. This causes satellite faces to have a chance of appearing in the equilibrium form.

5.3. *Faces perpendicular to a modulation wave vector with an incommensurate direction*

From §4.3, we have learned that one must study the $(0, 1)_s$ plane in the $(1+1)$-dimensional embedding of

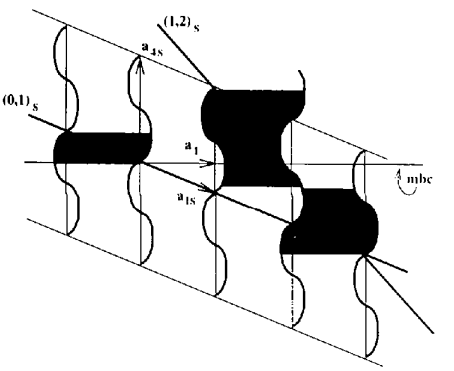

Fig. 8. Demonstration of the principle of selective cuts for the satellite faces (1112) and (0111). The situations can be represented with a $(1, 2)_s$ and $(0, 1)_s$ plane, respectively. The embedded m.b.c. is the same as in Fig. 7. The cut bonds have been shaded. It is clear that bonds of the m.b.c. are much more selectively cut by the (0111) plane than by the (1112) plane.

each and every m.b.c. in the crystal in the case of a face perpendicular to a $\mathbf{q}$ with an incommensurate direction. In §5.2, it has been shown for the (0111) plane that such a $(0, 1)_s$ plane is highly selective in cutting bonds when the corresponding value of q_1 is close to 0.35. The same applies, of course, here. However, the stabilization of the (0001) plane, which is considered here, can be larger than the stabilization of a plane like the (0111) plane. This is because in the case of the (0001) plane we must consider for each and every m.b.c. a $(0, 1)_s$ plane. On the other hand, for the (0111) plane, for example, this is the case for a m.b.c. with $\mathbf{b} = \mathbf{a}_1$ but, for a m.b.c. with $\mathbf{b} = \mathbf{a}_2$, the $(1, 1)_s$ plane and not the $(0, 1)_s$ would have to be considered. Of course, the value of $\mathbf{q} \cdot \mathbf{b}$ determines the degree of selectivity but, for any value of $\mathbf{q} \cdot \mathbf{b}$, the average energy of the embedded bonds cut by the $(01)_s$ plane is lower than the average energy of the bonds cut by the $(11)_s$ plane (see Kemers *et al.*, 1994, Fig. 5).

The amount of stabilization for the (0001) plane for a $\mathbf{q}$ with an incommensurate direction again depends on the modulation function, the modulation amplitude vector and the modulation wave vector as described in §5.1.

5.4. *Faces perpendicular to a modulation wave vector with an incommensurate length*

The largest possible stabilization is reached for a plane perpendicular to a $\mathbf{q}$ with an incommensurate length. This is because there is a two-dimensional lattice periodicity on this plane. Therefore, this is the only case in which a finite number of different bonds is cut.

In Fig. 9, this is demonstrated for $\mathbf{q} \| \mathbf{a}_1$, $\mathbf{f} \| \mathbf{a}_1$ and the m.b.c. for which $\mathbf{b} = \mathbf{a}_1$. It has been explained in §4.4 that one must average, in this case, over all intersection points of a $(0, 1)_s$ plane with a $(1, 0)_s$ grid in one unit cell of the lattice Λ_b on the plane $V_{\mathbf{b},s}$. Fig. 9 shows that for the chosen example only one bond is cut. Thus, the $(1, 0)_s$ grid and the $(0, 1)_s$ plane can be positioned such that precisely the longest bond is cut, which has the lowest energy possible for that bond. Of course, this gives the largest stabilization. This stabilization may be so large that (other) satellite faces loose their chance of appearing on the equilibrium morphology. In that case, only main faces determine the morphology together with this one exceptional face.

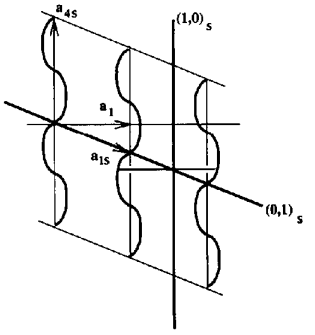

Fig. 9. Demonstration of the principle of selective cuts for the (1000) plane perpendicular to the vector $\mathbf{q} = q_1\mathbf{a}^*$. The bonds intersected by this plane in the physical crystal are found by the construction described in §4.4. In this case, only one bond is cut, which has been drawn. The (1000) plane is thus stabilized considerably.

Although it is equally possible to consider the plane perpendicular to a $\mathbf{q}$ with an incommensurate length as a satellite face, we choose to consider it as a main face because a face with the same orientation can be present on the crystal if the modulation is absent.

6. Model calculations

In order to obtain in our broken-bond model the surface free energy $\Gamma_{(h_1h_2h_3h_4)}$ for the plane $(h_1h_2h_3h_4)$, one must calculate, for each type of m.b.c. specified by the bond-chain vector $\mathbf{b}_i$, both the m.b.c. density $S_{\mathbf{b}_i}^{-1}$ on the plane and the average energy $\bar{\gamma}_{\mathbf{b}_i,(h_1h_2h_3h_4)}$ of all bonds, belonging to the m.b.c., that are cut by the (infinitely large) plane. The surface free energy is then given by

$$\Gamma_{(h_1h_2h_3h_4)} = \sum_{\mathbf{b}_i} S_{\mathbf{b}_i}^{-1} \bar{\gamma}_{\mathbf{b}_i,(h_1h_2h_3h_4)}, \tag{30}$$

where the summation is performed over all m.b.c.'s that are present in the crystal. If the crystal is not modulated, one should substitute $\gamma_{\mathbf{b}_i}$ for $\bar{\gamma}_{\mathbf{b}_i,(h_1h_2h_3h_4)}$ in (30) because the energies of the cut bonds are then not modulated. Moreover, there is, of course, no average that can depend on the indices h_1, h_2, h_3 and h_4.

The m.b.c. density $S_{\mathbf{b}_i}^{-1}$ is determined from the average surface area $S_{\mathbf{b}_i}$ on the plane for each m.b.c. of type $\mathbf{b}_i$. It is the same for both the modulated and the non-modulated crystal.

$$\begin{aligned} S_{\mathbf{b}_i}^{-1} &= n_i |\mathbf{b}_i \cdot \mathbf{H}_{(h_1h_2h_3h_4)}| / |\mathbf{H}_{(h_1h_2h_3h_4)}| \\ &= n_i |\mathbf{b}_i \cdot \mathbf{H}_{(h_1h_2h_3h_4)}| d_{(h_1h_2h_3h_4)}, \end{aligned} \tag{31}$$

where n_i is the average number of m.b.c.'s of type i per unit volume in the crystal.

The average energy $\bar{\gamma}_{\mathbf{b}_i}$ is calculated in superspace by using the one-to-one correspondence between (satellite) planes and crystallographic hyperplanes as has been outlined in §4. A numerical integration is performed over the energy of the bonds that are cut by the grid of net planes $(h_1h_2h_3h_4)_s$ within one unit cell of the lattice Λ_s in superspace. The energy γ of a bond is taken to be inversely proportional to the length l of the bond:

$$\gamma = \chi / l.$$

We take $\chi = 1$ in our calculations.

The dependence of $\Gamma_{(h_1h_2h_3h_4)}$ on the position of the plane within one $d_{(h_1h_2h_3h_4)}$ in the physical crystal is studied by calculating $\Gamma_{(h_1h_2h_3h_4)}$ for 750 equidistant planes $(h_1h_2h_3h_4)_s$ within one $d_{\mathbf{H},s}$ in superspace. It is important to realize that, for all m.b.c.'s $\mathbf{b}_i$, the average

energies $\bar{\gamma}_{\mathbf{b}_i}$ that are put in (30) must be calculated for the same position of the hyperplane in superspace. One of these positions will, thus, approximate the smallest surface free energy that is possible for this plane. We assume that the plane $(h_1h_2h_3h_4)$ always takes the corresponding position $(\mathrm{mod}\, d_{(h_1h_2h_3h_4)})$ in the physical crystal. Therefore, this minimal surface free energy for each face $(h_1h_2h_3h_4)$ is used for a standard Wulff plot in order to construct the equilibrium morphology.

When we are dealing with a modulation wave vector with an incommensurate length, a plane $(h_1h_2h_30)$, perpendicular to it, is treated separately in the way explained in §4.4. The positions of both the $(0001)_s$ plane and the grid of $(h_1h_2h_30)_s$ planes are varied over their corresponding $d_{\mathbf{H},s}$ in superspace in order to find the minimal surface free energy of this plane.

The surface free energies of planes $(h_1h_2h_3h_4)$ that one thus obtains only depend on the orientation of the plane. This means that a plane $(\bar{h}_1\bar{h}_2\bar{h}_3\bar{h}_4)$ has the same surface free energy as the plane $(h_1h_2h_3h_4)$. Furthermore, only planes have to be considered for which the indices have 1 as largest common divisor. In the model calculations that are presented in this paper, the maximum value used for h_1 and h_2 is 2, whereas for h_3 and h_4 it is 3.

The model crystal that we consider is an incommensurately modulated simple cubic crystal with only one kind of atom and three m.b.c.'s: $\mathbf{b}_1 = \mathbf{a}_1$, $\mathbf{b}_2 = \mathbf{a}_2$ and $\mathbf{b}_3 = \mathbf{a}_3$. The edges of the cubic unit cell of Λ have length 5 (units of length). The modulation wave function is $u(\tau) = \cos(\tau)$. We have chosen this model crystal because it is one of the simplest possible. Therefore, it allows one to study in detail the behaviour of the equilibrium morphology as a function of the length as well as the direction of both the modulation amplitude vector $\mathbf{f}$ and the modulation wave vector $\mathbf{q}$. The results are presented in the following subsections.

6.1. *The equilibrium morphology as a function of the direction of the modulation amplitude vector*

In Figs. 10, 11 and 12, the equilibrium morphology as obtained from a Wulff plot is shown for $\mathbf{f}||\mathbf{a}_1$, $\mathbf{f}||\mathbf{a}_2$ and $\mathbf{f}||\mathbf{a}_3$, respectively. The length of the modulation amplitude vector is $|\mathbf{f}| = 1.75$ (units of length) for all three figures. The modulation wave vector $\mathbf{q}$ has an incommensurate direction but is infinitely close to $0.6\mathbf{a}_1^* + 0.3\mathbf{a}_3^*$.

In Table 1, all faces are listed that occur on at least one of these three morphologies. The surface free energies of the faces are given for the case that the modulation amplitude is zero (non-modulated crystal) and for the three cases represented in Figs. 10, 11 and 12.

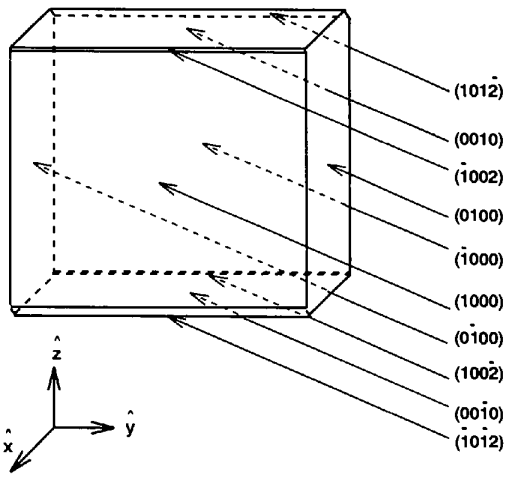

Fig. 11. Equilibrium morphology of an incommensurately modulated simple cubic crystal with only m.b.c.'s along the crystallographic axes. The modulation wave vector has an incommensurate direction but is infinitely close to $0.6\mathbf{a}_1^* + 0.3\mathbf{a}_3^*$. The modulation amplitude vector is $\mathbf{f} = (0, 0.35, 0)$.

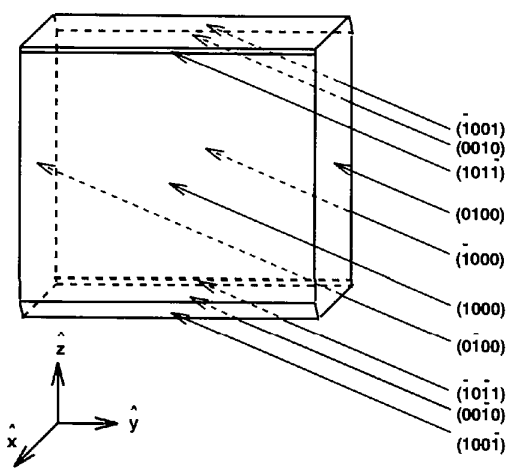

Fig. 10. Equilibrium morphology of an incommensurately modulated simple cubic crystal with only m.b.c.'s along the crystallographic axes. The modulation wave vector has an incommensurate direction but is infinitely close to $0.6\mathbf{a}_1^* + 0.3\mathbf{a}_3^*$. The modulation amplitude vector is $\mathbf{f} = (0.35, 0, 0)$.

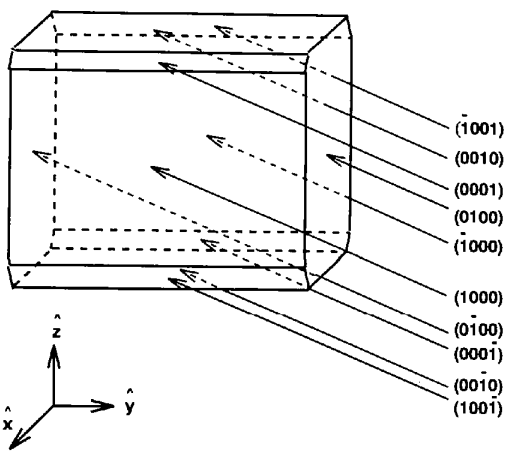

Fig. 12. Equilibrium morphology of an incommensurately modulated simple cubic crystal with only m.b.c.'s along the crystallographic axes. The modulation wave vector has an incommensurate direction but is infinitely close to $0.6\mathbf{a}_1^* + 0.3\mathbf{a}_3^*$. The modulation amplitude vector is $\mathbf{f} = (0, 0, 0.35)$.

Table 1. *Surface free energies and m.b.c. densities for important faces on the equilibrium morphologies of an incommensurately modulated simple cubic crystal with only m.b.c.'s along the crystallographic axes*

The four columns with surface free energies give the results for four different modulation amplitude vectors: $\mathbf{f} = 0$, $\mathbf{f} = (0.35, 0, 0)$, $\mathbf{f} = (0, 0.35, 0)$ and $\mathbf{f} = (0, 0, 0.35)$, respectively. The equilibrium morphologies of the latter three cases are given in Figs. 10, 11 and 12. A value of the surface free energy enclosed by a box indicates that the corresponding face appears in the equilibrium form of the crystal. The modulation wave vector has an incommensurate direction, but is infinitely close to $0.6\mathbf{a}_1^* + 0.3\mathbf{a}_3^*$.

Face	$\Gamma(\mathbf{f}=0)$	$\Gamma(\mathbf{f}\|\|\mathbf{a}_1)$	$\Gamma(\mathbf{f}\|\|\mathbf{a}_2)$	$\Gamma(\mathbf{f}\|\|\mathbf{a}_3)$	$S_{\mathbf{a}_1}^{-1}$	$S_{\mathbf{a}_2}^{-1}$	$S_{\mathbf{a}_3}^{-1}$
(1000)	0.0080	0.0059	0.0073	0.0073	1	0	0
(0100)	0.0080	0.0080	0.0080	0.0080	0	1	0
(0010)	0.0080	0.0075	0.0075	0.0066	0	0	1
(0001)	0.0107	0.0088	0.0098	0.0090	0.89	0	0.45
(100$\bar{1}$)	0.0112	0.0086	0.0100	0.0089	0.80	0	0.30
(101$\bar{1}$)	0.0109	0.0092	0.0101	0.0097	0.50	0	0.87
(101$\bar{2}$)	0.0107	0.0098	0.0093	0.0099	0.45	0	0.89
(100$\bar{2}$)	0.0101	0.0094	0.0093	0.0084	0.32	0	0.95
(0111)	0.0133	0.0122	0.0126	0.0120	0.34	0.57	0.74

Furthermore, the (0111) face has been added. Also, the m.b.c. densities $S_{\mathbf{a}_1}^{-1}$, $S_{\mathbf{a}_2}^{-1}$ and $S_{\mathbf{a}_3}^{-1}$ are given for all faces. The m.b.c. density does not depend on the modulation amplitude vector. It is therefore the same for all cases considered. The faces that appear on the equilibrium morphology are enclosed by boxes in Table 1. When there is no modulation ($\mathbf{f} = 0$), only the faces (1000), (0100) and (0010) appear and all have the same surface free energy. The equilibrium form is, therefore, a cube. When there is a modulation, the equilibrium morphology is different. Here, we describe the dependence of this morphology on the direction of the modulation amplitude vector.

In §5.1, it has been explained that the amount of stabilization for the energy $\bar{\gamma}_{\mathbf{b}}$ of a certain m.b.c. with bond vector $\mathbf{b}$ is expected to be larger if the value of $|\mathbf{f} \cdot \mathbf{b}|$ is larger. Furthermore, one knows from (30) that a larger m.b.c. density $S_{\mathbf{b}}^{-1}$ means that this stabilization is more effective in decreasing the surface free energy $\Gamma_{(h_1h_2h_3h_4)}$ of the plane. Therefore, the lowest surface free energy is expected if the modulation amplitude vector is parallel to the bond-chain vector of the m.b.c. that has the largest m.b.c. density. Table 1 shows that this is indeed the case for the planes (1000), (0010), (0001), (100$\bar{1}$), (100$\bar{2}$) and (0111). This, of course, also holds for many other planes that are not given in the table. Note that both main faces and satellite faces can be stabilized owing to the modulation. For the face (0100), the m.b.c. density is largest for $\mathbf{b} = \mathbf{a}_2$ but the corresponding m.b.c. is not modulated since $\mathbf{q} \cdot \mathbf{a}_2 = 0$ so that there can be no stabilization for $\bar{\gamma}_{\mathbf{a}_2}$. At this point, we must mention that a small technical problem still exists. For example, for the (1000) plane, the m.b.c. densities for $\mathbf{b} = \mathbf{a}_2$ and $\mathbf{b} = \mathbf{a}_3$ have been taken as zero, because $\mathbf{a}_2$ and $\mathbf{a}_3$ are parallel to the plane. However, owing to the displacement of the atoms due to the modulation, bonds of these m.b.c.'s can be cut for some special positions of the plane. Of course, these contribute to the total surface free energy. In this paper, however, we have neglected these cases but in a forthcoming paper we will present a solution to this small technical problem.

For the faces (101$\bar{1}$) and (101$\bar{2}$), the m.b.c. density is largest for $\mathbf{b} = \mathbf{a}_3$. Nevertheless, the stabilization of the surface free energy is not largest for $\mathbf{f}||\mathbf{a}_3$. In order to understand this, one must consider the $(1 + 1)$-dimensional embedding of the m.b.c.'s. For example, for the (101$\bar{1}$) plane, the grid $(1\bar{1})_s$ has to be considered for both the m.b.c. with $\mathbf{b} = \mathbf{a}_1$ and the m.b.c. with $\mathbf{b} = \mathbf{a}_3$. However, the corresponding values of q_1 in the $(1 + 1)$-dimensional embeddings equal $\mathbf{q} \cdot \mathbf{b}$, which is $q_1 = 0.6$ for $\mathbf{b} = \mathbf{a}_1$ and $q_1 = 0.3$ for $\mathbf{b} = \mathbf{a}_3$. In Fig. 5 of Kremers *et al.* (1994), it is shown that for $q_1 = 0.6$ the stabilization of the $(1\bar{1})_s$ plane is much larger than for $q_1 = 0.3$. This is the reason that, although the m.b.c. density is largest for $\mathbf{b} = \mathbf{a}_3$, $\Gamma_{(101\bar{1})}$ is lowest for $\mathbf{f}||\mathbf{a}_1$.

The importance of the $(1 + 1)$-dimensional embedding is further demonstrated by the fact that for $\mathbf{f}||\mathbf{a}_1$ the satellite faces (100$\bar{1}$) and (101$\bar{1}$) appear on the equilibrium form. For both of them, one must consider the grid $(1\bar{1})_s$ for the m.b.c. with $\mathbf{b} = \mathbf{a}_1$. The value of $\mathbf{q} \cdot \mathbf{b}$ is $q_1 = 0.6$, which is very favourable for $(1\bar{1})_s$. On the other hand, the satellite faces (0001) and (100$\bar{1}$) appear in the equilibrium form when $\mathbf{f}||\mathbf{a}_3$. For these faces, one must consider the grid $(01)_s$ for the m.b.c. with $\mathbf{b} = \mathbf{a}_3$. The value of $\mathbf{q} \cdot \mathbf{b}$ is $q_1 = 0.3$, which is very favourable for $(01)_s$ (see again Kremers *et al.*, 1994, Fig. 5).

In §5.3, it has been predicted that, in the case of a modulation wave vector with an incommensurate direction, the (0001) plane is stabilized more than the (0111) plane. The results in Table 1 confirm this prediction. The surface free energy of the (0111) plane is, for $\mathbf{f}||\mathbf{a}_3$, for example, 9.64% lower than its value for the non-modulated crystal. The surface free energy of the (0001) plane is, however, for the same $\mathbf{f}$ even 15.89% lower than its value for the non-modulated crystal. Indeed, (0001) is stabilized more than (0111) because in the case of (0001) only $(01)_s$ planes must be considered, whereas, for (0111), $(11)_s$ planes are also relevant.

The influence of the direction of $\mathbf{f}$ can now be summarized as follows. The largest stabilization for $\Gamma_{(h_1h_2h_3h_4)}$ can be expected if $|\mathbf{f} \cdot \mathbf{b}|$ is largest for the

Table 2. *Surface free energies Γ and m.b.c. densities S^{-1} for important faces on the equilibrium morphologies of an incommensurately modulated simple cubic crystal with only m.b.c.'s along the crystallographic axes*

The four columns with surface free energies give the results for four different lengths of the modulation amplitude vector parallel to $\mathbf{a}_2$: $|\mathbf{f}| = 0$, $|\mathbf{f}| = 0.5$, $|\mathbf{f}| = 1.0$ and $|\mathbf{f}| = 2.25$, respectively. A value of the surface free energy enclosed by a box indicates that the corresponding face appears in the equilibrium form of the crystal. The modulation wave vector has an incommensurate direction, but is infinitely close to $0.6\mathbf{a}_1^* + 0.3\mathbf{a}_3^*$.

Face	$\Gamma(\mathbf{f}=0)$	$\Gamma(\lvert\mathbf{f}\rvert=0.5)$	$\Gamma(\lvert\mathbf{f}\rvert=1.0)$	$\Gamma(\lvert\mathbf{f}\rvert=2.25)$	$S^{-1}_{\mathbf{a}_1}$	$S^{-1}_{\mathbf{a}_2}$	$S^{-1}_{\mathbf{a}_3}$
(1000)	0.0080	0.0079	0.0077	0.0069	1	0	0
(0100)	0.0080	0.0080	0.0080	0.0080	0	1	0
(0010)	0.0080	0.0079	0.0078	0.0072	0	0	1
$(10\bar{1}2)$	0.0107	0.0106	0.0102	0.0087	0.45	0	0.89
$(20\bar{1}2)$	0.0107	0.0106	0.0104	0.0093	0.89	0	0.45
$(100\bar{2})$	0.0107	0.0100	0.0098	0.0089	0.32	0	0.95
(1200)	0.0107	0.0107	0.0106	0.0102	0.45	0.89	0
$(1\bar{2}00)$	0.0107	0.0107	0.0106	0.0102	0.45	0.89	0
(0210)	0.0107	0.0107	0.0106	0.0103	0	0.89	0.45
$(02\bar{1}0)$	0.0107	0.0107	0.0106	0.0103	0	0.89	0.45

m.b.c. that is most effective. This effectiveness can be increased by both a large m.b.c. density and a favourable value of $q_1 = \mathbf{q} \cdot \mathbf{b}$ for the grid $(h_1 b_1 + h_2 b_2 + h_3 b_3, h_4)_s$ that must be considered for this plane.

6.2. *The equilibrium morphology as a function of the length of the modulation amplitude vector*

In this section, we present calculations on the equilibrium morphology of the same simple cubic crystal as in §6.1. The modulation wave vector again is $\mathbf{q} = 0.6\mathbf{a}_1^* + 0.3\mathbf{a}_3^*$ and the modulation amplitude vector $\mathbf{f}$ is parallel to $\mathbf{a}_2$. The surface free energies have been calculated for three different lengths of the modulation amplitude vector: $|\mathbf{f}| = 0.5$, $|\mathbf{f}| = 1.0$ and $|\mathbf{f}| = 2.25$. The results are given in Table 2 and the faces that appear on the equilibrium morphology are enclosed by a box. In addition, the surface free energies for the non-modulated crystal are given and also the m.b.c. densities for the three m.b.c.'s that are present in the crystal.

It is clear that for all faces the stabilization increases with the modulation amplitude, as expected. Moreover, the larger the modulation amplitude, the more faces that can appear in the equilibrium morphology. This is caused by the fact that the dependence on the modulation amplitude can be different for different faces. For example, the satellite face $(10\bar{1}2)$ and the main face (0210) have equal surface free energy for $|\mathbf{f}| = 0$. For $|\mathbf{f}| \neq 0$, however, the surface free energy is smaller for the $(10\bar{1}2)$ face than for the (0210) face.

In order to explain this, we consider the $(1+1)$-dimensional embedding of a m.b.c. consisting of one type of atom and one type of bond, $u(\tau) = \cos(\tau)$ and $\mathbf{f} \| \mathbf{b}$. One can easily derive that the (largest) average length of the embedded bonds cut by a $(10)_s$ plane is

$$\bar{l}_{(10)_s} = |\mathbf{b}| + 4|\mathbf{f}|(1 - \cos q_1).$$

On the other hand, the (largest) average length of the bonds cut by a $(01)_s$ plane is

$$\bar{l}_{(01)_s} = |\mathbf{b}| + (2/q_1)|\mathbf{f}|(1 - \cos q_1)$$

and the (largest) average length of the bonds cut by a $(1\bar{1})_s$ plane is

$$\bar{l}_{(1\bar{1})_s} = |\mathbf{b}| + [2/(1 - q_1)]|\mathbf{f}|(1 - \cos q_1).$$

Note that in all cases the average length increases linearly with $|\mathbf{f}|$ but the value of q_1 determines which proportionality constant is larger. For $q_1 < 0.5$, the average length is largest for the $(01)_s$ plane, smallest for the $(1\bar{1})_s$ plane and the value for the $(10)_s$ plane is in between. For $q_1 > 0.5$, this order is reversed.

In Table 2, it can be seen that the dependence of the surface free energy on the modulation amplitude is stronger for (1000) than for (0010). The reason for this difference lies exactly in the fact that for the (1000) plane a $(10)_s$ plane must be considered with $q_1 = 0.6$, whereas for the (0010) plane a $(10)_s$ plane must be considered with $q_1 = 0.3$. For $q_1 = 0.6$, the average length of the cut bonds is larger than for $q_1 = 0.3$. Therefore, the (1000) plane is stabilized more than the (0010) plane.

The sensitivity of the amount of stabilization for the length of the modulation amplitude vector is thus determined by (among others) the values of $q_1 = \mathbf{q} \cdot \mathbf{b}$ for the $(1+1)$-dimensional embeddings of the m.b.c.'s present in the crystal. The influence of the modulation amplitude is, therefore, not independent of the modulation wave vector. Which faces appear on the equilibrium shape with increasing $|\mathbf{f}|$ is thus mainly determined by the modulation wave vector $\mathbf{q}$. However, in general, one can say that more faces can appear if $|\mathbf{f}|$ is larger.

6.3. *The equilibrium morphology as a function of the length of the modulation wave vector*

From §§6.1 and 6.2, we have learned that the values of $q_1 = \mathbf{q} \cdot \mathbf{b}$ for the $(1+1)$-dimensional embeddings of the m.b.c.'s that are present in the crystal are essential parameters for the equilibrium morphology. These values depend, of course, on the length of the modulation wave vector. Therefore, three additional model calculations have been performed for the simple cubic crystal with

Table 3. *Surface free energies for important faces on the equilibrium morphologies of an incommensurately modulated simple cubic crystal with only m.b.c.'s along the crystallographic axes*

The four columns with surface free energies give the results for four different lengths of the modulation wave vector. In all cases, the modulation amplitude vector is $\mathbf{f} = (0, 0.2, 0)$. A value of the surface free energy enclosed by a box indicates that the corresponding face appears in the equilibrium form of the crystal. The modulation wave vector has in all cases an incommensurate direction infinitely close to $\mathbf{q} = (2\gamma, 0, \gamma)$.

Face	$\Gamma(\mathbf{q} = (0.4, 0, 0.2))$	$\Gamma(\mathbf{q} = (0.6, 0, 0.3))$	$\Gamma(\mathbf{q} = (0.8, 0, 0.4))$	$\Gamma(\mathbf{q} = (0.9, 0, 0.45))$
(1000)	0.0077	0.0077	0.0079	0.0080
(0100)	0.0080	0.0080	0.0080	0.0080
(0010)	0.0079	0.0078	0.0077	0.0077
(0001)	0.0104	0.0104	0.0105	0.0106
(101$\bar{2}$)	0.0098	0.0102	0.0098	0.0088
(100$\bar{1}$)	0.0098	0.0108	0.0104	0.0092
(100$\bar{2}$)	0.0105	0.0098	0.0109	0.0110
(201$\bar{2}$)	0.0104	0.0104	0.0105	0.0105

$\mathbf{f} = (0, 0.2, 0)$ and a modulation wave vector $\mathbf{q}$ with the same incommensurate direction as used in §6.2 but having different lengths. The results are summarized in Table 3.

It can be observed clearly that those faces appear in the equilibrium morphology for which there exist favourable $q_1 = \mathbf{q} \cdot \mathbf{b}$ values for the $(h_1 b_1 + h_2 b_2 + h_3 b_3, h_4)_s$ planes in the $(1 + 1)$-dimensional embeddings of the m.b.c.'s.

6.4. *The equilibrium morphology as a function of the direction of the modulation wave vector*

So far, we have only considered modulation wave vectors with an incommensurate direction. However, as explained in §5.4, one expects that faces perpendicular to a modulation wave vector with an incommensurate length can be stabilized more by the modulation than all other possible faces. Therefore, model calculations have been performed for the simple cubic crystal with $\mathbf{f} = (0, 0.2, 0)$ and three different directions for the modulation wave vector, infinitely close to $\mathbf{q} = (0, 0, 0.3)$, $\mathbf{q} = (0.6, 0, 0.3)$ and $\mathbf{q} = (0.1, 0.2, 0.3)$. All these $\mathbf{q}$ vectors are taken to have an incommensurate length. The faces perpendicular to these $\mathbf{q}$ vectors are (0010), (2010) and (1230), respectively. The morphologies are presented in Figs. 13, 14 and 15.

The surface free energies of the faces appearing in Fig. 14 for the case where $\mathbf{q} = 0.6\mathbf{a}_1^* + 0.3\mathbf{a}_3^*$ are given in Table 4.

These results should be compared with the ones given in Table 2 for $|\mathbf{f}| = 1.0$ because, besides the character of the modulation wave vector, this is the same crystal. It is very clear that, only when $\mathbf{q}$ has an incommensurate length, is the face (2010) perpendicular to it stabilized so much that it appears in the equilibrium morphology.

Furthermore, the direction of $\mathbf{q}$, of course, determines the values of $q_1 = \mathbf{q} \cdot \mathbf{b}$ in the $(1 + 1)$-dimensional embeddings of the m.b.c.'s. As we know already, a change of these values can change the equilibrium morphology considerably. Again, this is demonstrated by the differences between Figs. 13, 14 and 15.

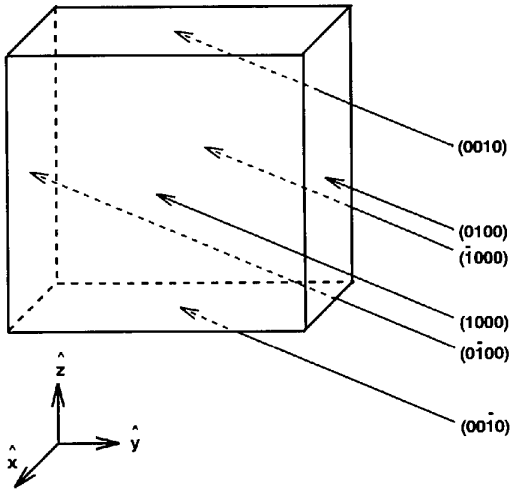

Fig. 13. Equilibrium morphology of an incommensurately modulated simple cubic crystal with only m.b.c.'s along the crystallographic axes. The modulation wave vector has an incommensurate length $\mathbf{q} = 0.3\mathbf{a}_3^*$. The plane perpendicular to $\mathbf{q}$ is (0010). The modulation amplitude vector is $\mathbf{f} = (0, 0.2, 0)$.

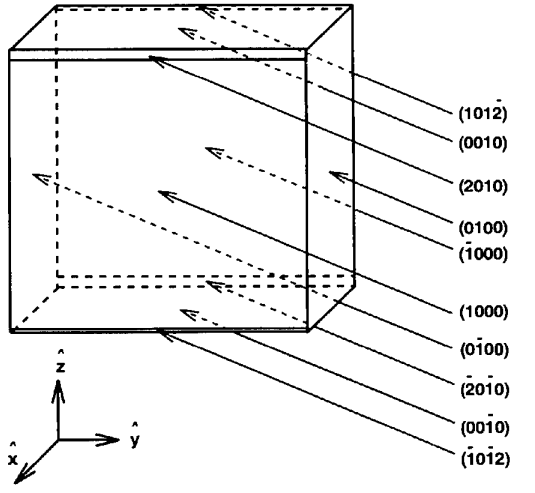

Fig. 14. Equilibrium morphology of an incommensurately modulated simple cubic crystal with only m.b.c.'s along the crystallographic axes. The modulation wave vector has an incommensurate length $\mathbf{q} = 0.6\mathbf{a}_1^* + 0.3\mathbf{a}_3^*$. The plane perpendicular to $\mathbf{q}$ is (2010). The modulation amplitude vector is $\mathbf{f} = (0, 0.2, 0)$.

Table 4. *Surface free energies for the faces on the equilibrium morphology of an incommensurately modulated simple cubic crystal with only m.b.c.'s along the crystallographic axes*

The modulation wave vector is $\mathbf{q} = 0.6\mathbf{a}_1^* + 0.3\mathbf{a}_3^*$. It has an incommensurate length. The modulation amplitude vector is $\mathbf{f} = (0, 0.2, 0)$. A value of the surface free energy enclosed by a box indicates that the corresponding face appears in the equilibrium form of the crystal.

Face	$\Gamma(\mathbf{q} = (0.6, 0, 0.3))$
(1000)	0.0077
(0100)	0.0080
(0010)	0.0078
(101$\bar{2}$)	0.0102
(2010)	0.0102

6.5. *The equilibrium morphology as a function of the modulation function*

In order to study the influence of the modulation function u on the equilibrium morphology, it is perhaps best to consider Fig. 5 of Kremers *et al.* (1994). The modulation function used for the calculation of that figure is $u(\tau) = \cos(\tau)$. In this paper, we have often refered to this figure because it gives the information of the average energy of the bonds cut by an $(h_1b_1 + h_2b_2 + h_3b_3, h_4)_s$ plane in the $(1+1)$-dimensional embedding of a m.b.c. However, if the modulation function is different, the shapes of the curves in this figure change.

In Fig. 16, the result is presented of a similar calculation, but in this case the modulation function is a square wave: $u(\tau) = f$ for $\tau \in [0, \frac{1}{2})$ and $u(\tau) = -f$ for $\tau \in [\frac{1}{2}, 1)$. It is very instructive to see that, for example, for the plane $(1\bar{1})_s$, a constant average energy is found for the cut bonds if $q_1 > 0.5$. This is in sharp contrast with the case of the modulation function $u(\tau) - \cos(\tau)$, for which a relatively sharp dip can be discovered for $q_1 = 0.65$. $(1\bar{1})_s$ planes will, of course, often be relevant for satellite planes $(h_1h_2h_3\bar{1})$ with at least one of the h_1, h_2 or h_3 equal to one. Therefore, for a block wave modulation, there will be many more m.b.c.'s with favourable $q_1 = \mathbf{q} \cdot \mathbf{b}$ values for the $(1\bar{1})_s$ planes than in the case of a sinusoidal modulation. The same kind of reasoning applies to the $(01)_s$ plane, which is of course also often relevant for satellite planes. Furthermore, it is very interesting that for the plane $(10)_s$ the dip in average energy at $q_1 = 0.5$ is much sharper for the square-wave modulation than for the sinusoidal modulation. $(10)_s$ planes will, of course, often be relevant for main planes $(h_1h_2h_30)$ with at least one of the h_1, h_2 or h_3 equal to one. Therefore, in the case of a square-wave modulation, there will be fewer m.b.c.'s with favourable $q_1 = \mathbf{q} \cdot \mathbf{b}$ values for the $(10)_s$ planes than in the case of a sinusoidal modulation.

The influence of the modulation function u can now be summarized as follows. If the modulation function resembles a square-wave function, one expects satellite planes to be stabilized more and main planes to be stabilized less as compared with the case when the modulation wave resembles a sinusoidal behaviour.

7. Discussion

In this paper, we have presented a broken-bond model for the calculation of surface free energies $\Gamma_{(h_1h_2h_3h_4)}$ for (satellite) planes $(h_1h_2h_3h_4)$ on incommensurately modulated crystals. Owing to the incommensurateness, it is, in general, not possible to define a mesh area $M_{(h_1h_2h_3h_4)}$ on such planes. In consequence, surface free energies have been calculated by averaging over infinite planes. One of

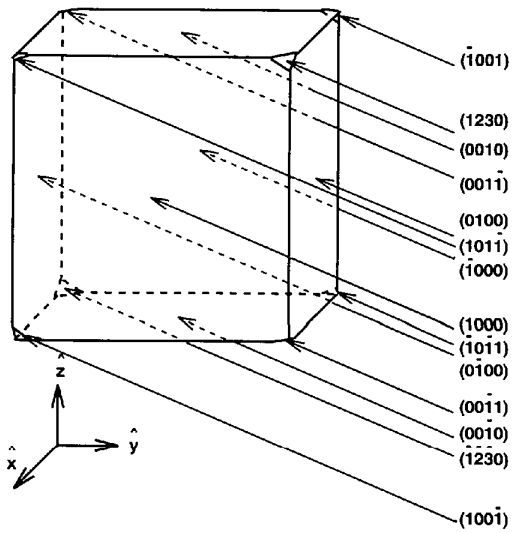

Fig. 15. Equilibrium morphology of an incommensurately modulated simple cubic crystal with only m.b.c.'s along the crystallographic axes. The modulation wave vector has an incommensurate length $\mathbf{q} = 0.1\mathbf{a}_1^* + 0.2\mathbf{a}_2^* + 0.3\mathbf{a}_3^*$. The plane perpendicular to $\mathbf{q}$ is (1230). The modulation amplitude vector is $\mathbf{f} = (0, 0.2, 0)$.

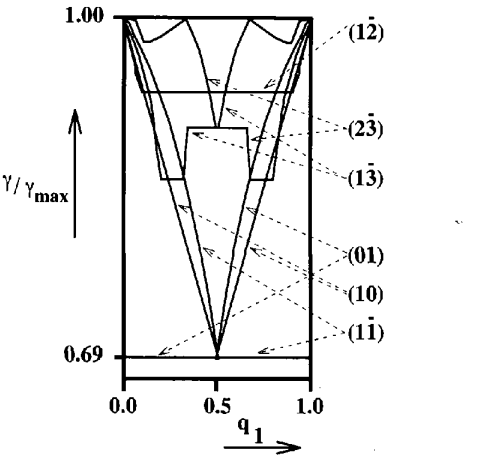

Fig. 16. Normalized minimal average energies $\gamma/\gamma_{\max}$ of the bonds cut by $(h_1b_1 + h_2b_2 + h_3b_3, h_4)_s$ planes in a $(1+1)$-dimensional embedding of a m.b.c. consisting of one type of atom. The modulation function u has a square-wave behaviour. The modulation amplitude is $f = 0.2b$.

the key assumptions is, then, that the surface free energies $\Gamma_{(h_1h_2h_3h_4)}$ thus obtained have the same meaning for the morphology as surface free energies $\Gamma_{(h_1h_2h_3)}$ for non-modulated crystals. With such an assumption, it is possible to calculate equilibrium morphologies by using these surface free energies $\Gamma_{(h_1h_2h_3h_4)}$ for a Wulff plot. This plot is intended to give a crystal shape that has minimal total surface free energy. The assumption can, therefore, be expected to be valid if the planes on the equilibrium shape are not too small. In our opinion, even micrometre-sized crystals already have faces so large that the difference between the actual average surface free energy and $\Gamma_{(h_1h_2h_3h_4)}$ for the infinite plane is negligible.

By means of a superspace approach, it has been shown that both main faces and satellite faces can be stabilized owing to the principle of selective cuts. van Smaalen (1993) has shown, using a different approach, that this can be understood to be a result of 'surface pinning of the phase of the modulation wave'. In order to make an estimate of the possible amount of stabilization for an actual incommensurately modulated crystal, we consider the example of the mineral calaverite $AuTe_2$. The modulation amplitude is about 0.4 Å for the Te atoms and the average length of the crystallographic axes $\mathbf{a}_1$, $\mathbf{a}_2$ and $\mathbf{a}_3$ is 5.4 Å (Schutte & de Boer, 1988). It seems reasonable to compare this with the case $|\mathbf{f}| = 0.5$ and $|\mathbf{a}| = 5$ for the simple cubic crystal in Table 2. In this way, we estimate that the surface free energy for faces appearing on $AuTe_2$ is of the order of 1% less than what it would be without the influence of the modulation, assuming the potential used to be relevant.

It is striking that, as a consequence, in a Wulff plot highly singular cusps appear in the polar plot of the surface free energies. For (low-index) main faces, there still exists a cusp in the Wulff plot, having the same shape as for the non-modulated crystal. However, at the centre of the cusp, the Wulff plot is discontinuous, contrary to the non-modulated case. This centre, being exactly one point, is displaced (by the order of 1%) towards the origin of the Wulff plot. There are, of course, many high-index planes that have face normals pointing to a position somewhere in the cusp. However, their indices are in general so high that there is virtually no stabilization for these planes as a result of the modulation. The shape of the cusp is, therefore, not altered at that position.

However, for a satellite face, the shape of the cusp is different. If the crystal were non-modulated, the polar plot of the surface free energy would have a convex shape in the direction of the face normal. The only change due to the modulation is that again exactly one point is displaced towards the origin, so that for a satellite face also the Wulff plot is discontinuous. A similar result has been obtained by van Smaalen (1993).

These singular cusps for both main and satellite faces seem to indicate that a finite amount of energy is necessary for any tilt of the surface of a face, however small. At present, it is unclear to us whether this has any physical relevance.

The presented analysis has shown that the surface free energy $\Gamma_{(h_1h_2h_3h_4)}$ depends, for a given crystal, on both the orientation of the plane (defined by $\mathbf{H}_{(h_1h_2h_3h_4)}$) and the position of the plane with respect to the origin. It is interesting that, with one exception, for all planes there exists a periodicity in the surface free energy. The period length is exactly $d_{(h_1h_2h_3h_4)}$. This can be considered as a generalization of the situation for non-modulated crystals, where this period length is $d_{(h_1h_2h_3)}$. Consequently, there is, for non-modulated crystals, within each distance $d_{(h_1h_2h_3)}$, a position of minimal surface free energy. It is common to assume that the plane takes exactly this position when it bounds the crystal. Therefore, the minimal surface free energy is used for a Wulff plot. For (satellite) planes on incommensurately modulated crystals, the situation can be considered to be no different. Within each distance $d_{(h_1h_2h_3h_4)}$, there exists a position of minimal surface free energy. It can thus be assumed that an $(h_1h_2h_3h_4)$ plane takes this position and that the corresponding minimal surface free energy is to be used in a Wulff plot. The exception is, of course, the plane perpendicular to a modulation wave vector that has an incommensurate length. For this plane, there is no positional periodicity in the surface free energy. Nevertheless, in the Wulff plot we have again taken the minimal surface free energy that could be found for the plane. This can be justified by assuming that the phase of the modulation wave can be pinned to a surface that bounds the crystal. It is well known that, for example, defects can pin the phase of the modulation wave. The surface of a crystal can be considered to be an intrinsic defect.

There is a further interesting aspect of the positional periodicity in the surface free energy because for non-modulated crystals it is believed that this periodicity is one of the main reasons that crystals grow with layers of thickness $d_{(h_1h_2h_3)}$. Although the analysis presented in this paper is not meant to explain the growth mechanism of (satellite) faces on incommensurately modulated crystals, we feel that the positional periodicity in $\Gamma_{(h_1h_2h_3h_4)}$, together with the fact that all slices $(h_1h_2h_3h_4)$ have the same energy content, should be considered as a serious indication for the possibility of a layer growth mechanism. We would like to stress that the growth of satellite faces on incommensurately modulated crystals cannot be viewed as more extraordinary than the growth of main planes. The first experimental indications of a layer growth mechanism have been reported by Dam (1985), who observed growth spirals on the satellite face $(10\bar{1}2)$ of a crystal of $[(CH_3)_4N]_2ZnCl_4$. It would be very interesting to measure the height of steps on (satellite) faces in order to see whether these steps are built of layers with thickness $d_{(h_1h_2h_3h_4)}$. Furthermore, one could expect that the face perpendicular to a modulation wave vector with an incommensurate length shows exceptional

growth behaviour because for such a face there does not exist a positional periodicity in the surface free energy.

The energy content E_H of a slice can be found in the following way. One divides every bond in the crystal in equal infinitesimal pieces that all have the same infinitesimal energy content dE. This is done in such a way, of course, that integrating the energies dE over the bond gives exactly the bond energy. E_H can then be calculated by integrating all those energies dE that correspond to the intersection of an $(h_1h_2h_3h_4)$ plane with a bond, for all positions of the plane within the slice. For such a calculation, a similar superspace approach can be used as for the calculation of surface free energies. This energy E_H includes the energy of the bond pieces within the slice that are part of the bonds that are intersected by the surfaces of the slice. If one omits the contributions of these bond pieces to E_H, the so-called quantity E_{slice} is found. This quantity is of importance for the crystal growth theory of non-modulated crystals (Bennema & van der Eerden, 1987). It thus differs from E_H. Nevertheless, one can calculate E_{slice} also for modulated crystals by subtracting the surface free energy $\Gamma_{(h_1h_2h_3h_4)}$ from E_H (and taking the appropriate units and dimensions into account, of course). The dependence of E_H and E_{slice} on the modulation properties has not been considered in this paper. However, it may be of importance for the growth of modulated crystals.

It has to be remarked that all calculations presented in this paper are essentially for zero temperature. For finite temperatures, one is faced with additional problems. It is well known that faces on non-modulated crystals have a roughening temperature T_R. Below T_R, the face is flat and there is a finite step free energy. However, at T_R there is a phase transition (of infinite order) at which the step free energy becomes zero. The face roughens because steps can be created without cost. The face can then no longer be uniquely identified. Consequently, one only takes those faces into account that have a roughening temperature higher than the actual temperature. In the case of incommensurately modulated crystals, it is even not known yet whether a roughening transition exists, although we want to mention the work of Dam (1985) who observed the roughening of a 'satellite' face upon a change of the modulation wave vector from one commensurate value to another. Nevertheless, from an experimental point of view, it is clear that both flat main faces and flat satellite faces do show up. This means that, if there is a roughening transition, there will be (satellite) faces that have a non-zero T_R. Moreover, if such a roughening transition is related to the step free energy, one could use the same lines of thought as presented in this paper for the calculation of these step free energies by making use of the embedding of the crystal in superspace. On the other hand, one can expect that $(h_1h_2h_3h_4)$ planes for which there exists a zero step free energy are in any case roughened, for the same reasons as $(h_1h_2h_3)$ planes are in non-modulated crystals.

It would, therefore, be sensible to check whether there are faces for which the step free energy is zero. This can be done analogously to the procedure that is commonly used for non-modulated crystals (Hartman & Perdok, 1955). First, the crystal is represented by a graph. The vertices of the graph represent the growth units and the connections between the vertices represent the bonds. However, in the graph there is no information about the energies of the bonds. For non-modulated crystals, it is then checked whether within an $(h_1h_2h_3)$ slice of thickness $d_{(h_1h_2h_3)}$ a connected net can be defined. A connected net is a two-dimensional net in which all vertices are connected with each other. The edge free energy for the face $(h_1h_2h_3)$ is expected to be zero in the case that it is not possible to find such a connected net. The graph of an incommensurately modulated crystal is equal to the graph of the same crystal without modulation if one assumes that due to the modulation no bonds disappear and no extra bonds appear. It follows that one can neglect the modulation for checking the connectedness of nets. It has been shown that an incommensurately modulated crystal can be partitioned in slices $(h_1h_2h_3h_4)$ with thickness $d_{(h_1h_2h_3h_4)}$ so that all have an equal energy content. Therefore, it seems justified to search for connected nets in precisely such slices. If there is no connected net, the face $(h_1h_2h_3h_4)$ can be expected to have a zero edge free energy. It will then be rough. Such an approach has been used by Vogels, Balzuweit, Meekes & Bennema (1992).

In this paper, we have studied the influence of the length and the direction of both the modulation wave vector and the modulation amplitude vector on the (equilibrium) morphology. Also, the influence of the modulation function has been outlined. The results obtained now allow us to obtain a first understanding of the differences in morphology of two well known incommensurate crystals, $[(CH_3)_4N]_2ZnCl_4$ and $AuTe_2$.

Crystals of $[(CH_3)_4N]_2ZnCl_4$ that have been grown at a temperature for which the structure is incommensurate almost always show only main faces. Several satellite faces can be observed, however, if a sphere growth experiment is performed (Dam, 1986; Vogels, Verheijen, Meeks & Bennema, 1992). In such an experiment, a single crystal is polished into a spherical shape, which is subsequently exposed to a slightly supersaturated solution so that it grows for a short time. All stable faces then show up as small flat regions on the sphere. On the other hand, the sphere roughens up in the regions where no stable faces are present. The incommensurate phase of $[(CH_3)_4N]_2ZnCl_4$ can be characterized with an orthorhombic lattice A, $|\mathbf{a}_1| = 12.258$, $|\mathbf{a}_2| = 8.987$ and $|\mathbf{a}_3| = 15.503$ Å (Madariaga, Zuñigo, Pérez-Mato & Tello, 1987). Furthermore, the modulation wave vector $\mathbf{q} \simeq 0.4\mathbf{a}_3^*$ can be assumed to have an incommensurate length and the modulation amplitude vector with maximum length is $\mathbf{f} \simeq 0.047\mathbf{a}_2$ for one of the chlorine atoms. For a large temperature region in the incommen-

surate phase, it is a reasonable assumption to take the modulation function as sinusoidal.

Contrary to the case of $[(CH_3)_4N]_2ZnCl_4$, numerous as well as large satellite faces can be found on as-grown crystals of $AuTe_2$, both for mineral crystals found in nature (Dam *et al.*, 1985) and for synthetically prepared crystals (Balzuweit, Meekes & Bennema, 1991). The incommensurate structure of $AuTe_2$ can be characterized with a monoclinic lattice A, $\beta = 90.038°$, $|\mathbf{a}_1| = 7.1947$, $|\mathbf{a}_2| = 4.4146$ and $|\mathbf{a}_3| = 5.0703$ Å (Schutte & de Boer, 1988). The modulation wave vector $\mathbf{q} \simeq -0.4076\mathbf{a}_1^* + 0.4479\mathbf{a}_3^*$ can be assumed to have an incommensurate direction and the largest modulation amplitude vector $|\mathbf{f}| \simeq 0.4$ Å is found for the Te atoms. The modulation functions for the different atoms contain first-, second- and third-order harmonics.

From these structural data, we can already obtain a fairly good understanding of why satellite faces appear much more easily on crystals of $AuTe_2$ than on crystals of $[(CH_3)_4N]_2ZnCl_4$. The analysis presented in this paper has shown that the appearance of satellite faces is favoured by a large modulation amplitude, a modulation wave vector with an incommensurate direction and a modulation function that resembles a square-wave behaviour. With respect to all these three aspects, $AuTe_2$ indeed has a more favourable structure than $[(CH_3)_4N]_2ZnCl_4$. The modulation amplitude of $AuTe_2$ is larger with respect to the lengths of the crystallographic axes than the modulation amplitude of $[(CH_3)_4N]_2ZnCl_4$. In addition, the modulation wave vector of $[(CH_3)_4N]_2ZnCl_4$ has an incommensurate length. Therefore, the {0010} faces perpendicular to it may be stabilized so much that they dominate the morphology and that, consequently, satellite faces do not appear. In the case of $AuTe_2$, the modulation wave vector has an incommensurate direction, so that there is no face perpendicular to the modulation wave vector that can dominate the morphology. Furthermore, the modulation functions for the atoms in $AuTe_2$ can be considered to be in closer resemblance with a square-wave behaviour than the modulation functions for the atoms in $[(CH_3)_4N]_2ZnCl_4$. Therefore, the relative stabilization of satellite faces with respect to the stabilization of main faces is expected to be larger for $AuTe_2$ than for $[(CH_3)_4N]_2ZnCl_4$. Note that a discussion along the same lines has been given by van Smaalen (1993).

In order to obtain a more complete insight into the differences in morphology for $AuTe_2$ and $[(CH_3)_4N]_2ZnCl_4$, one should perform calculations as described in §6 using reasonable choices of bonds that build m.b.c.'s. Such calculations will be presented in a forthcoming paper.

Finally, we would like to point out that the superspace approach, which has been used here, is not restricted to incommensurate displacively modulated three-dimensional crystals. Instead of taking modulated positions that define modulated bonds, one can also take only modulated bond energies and leave the positions unaffected by the modulation. The same kind of theory applies as outlined in §4 and the same kind of computer program is needed to calculate surface free energies numerically. Of course, also incommensurately modulated two-dimensional crystals can be dealt with using a similar superspace approach.

Another, very interesting, class of crystals is formed by the incommensurate composite crystals. These crystals can also be embedded in a superspace (Janner & Janssen, 1980; van Smaalen, 1992). Here, we will not go into detail but they may be considered as a collection of incommensurately modulated crystals. So far, little attention has been paid to the morphology of these crystals. It will be clear that the analysis presented in this paper immediately applies to each incommensurately modulated crystal from the collection that builds the incommensurate composite crystal. Special attention must be paid to bonds between atoms belonging to different incommensurately modulated structures from the collection. However, since incommensurate composite crystals can be embedded, we are confident that the superspace approach for the morphology can be extended to the case of these crystals.

There is still another class of incommensurate crystals that can be described using an embedding in a superspace. This class is formed by the so-called quasicrystals. The Fibonacci chain of atoms is a famous example of a one-dimensional quasicrystal. It has been shown by Heijmen *et al.* (1994) that the morphology of this chain can be dealt with in a superspace approach. In a forthcoming paper (Heijmen *et al.*, 1995), it will be shown that the same holds for quasiperiodic tilings.

In summary, one can say that the superspace approach for morphology is promising for all classes of incommensurate crystals.

8. Concluding remarks

It has been shown that in an incommensurately modulated crystal one can define modulated bond chains that are characterized by a bond-chain vector **b**. By means of the $(3 + 1)$-dimensional embedding of the modulated crystal in superspace, it is found that $(1 + 1)$-dimensional embeddings can be defined for these m.b.c.'s. The corresponding value for q_1 depends on the actual modulation wave vector **q** and on the bond-chain vector **b**, $q_1 = \mathbf{q} \cdot \mathbf{b}$. The bonds of the m.b.c.'s that are intersected by a (satellite) plane $(h_1h_2h_3h_4)$ in the physical crystal can be found by intersecting the uniform bond density in superspace with an $(h_1b_1 + h_2b_2 + h_3b_3, h_4)_s$ grid in the $(1 + 1)$-dimensional embedding of the m.b.c. Moreover, it has been shown that these are also exactly the bonds that are intersected by a crystallographic hyperplane in superspace. Therefore, one can state that there is a one-to-one correspondence between crystallographic hyperplanes $(h_1h_2h_3h_4)_s$

and (satellite) planes $(h_1h_2h_3h_4)$ in the physical crystal as far as the morphology is concerned. This correspondence gives the possibility of calculating numerically average surface free energies $\Gamma_{(h_1h_2h_3h_4)}$ by means of a superspace approach for arbitrarily complex incommensurately modulated structures.

In the $(1+1)$-dimensional embeddings of m.b.c.'s, one can see immediately that there is a principle of selective cutting. A (satellite) plane $(h_1h_2h_3h_4)$ in the physical crystal intersects only a selection of the infinite number of different bonds that exist due to the modulation. The (satellite) plane can be positioned such that the plane is stabilized with respect to the non-modulated crystal. This explains the occurrence of satellite planes in incommensurately modulated crystals. In principle, planes perpendicular to a modulation wave vector with an incommensurate length can be stabilized more than satellite planes perpendicular to a modulation wave vector with an incommensurate direction. The latter can have, however, more stabilization than other satellite planes. These, in turn, can be stabilized more than main planes non-perpendicular to the modulation wave vector. Generally, it can be said that the amount of stabilization depends on the length of the mesh area of the one-dimensional $(h_1b_1 + h_2b_2 + h_3b_3, h_4)_s$ plane. Therefore, low-index planes can be stabilized more than high-index planes in correspondence with the classical case.

Furthermore, it has been found that an incommensurately modulated crystal can be partitioned, for any orientation $(h_1h_2h_3h_4)$, in slices of thickness $d_{(h_1h_2h_3h_4)}$ that have the same energy content and the same surface free energy. This can be seen as a generalization of the situation in non-modulated crystals. There is one exception, which is the case of a plane perpendicular to a modulation wave vector that has an incommensurate length.

The surface free energies $\Gamma_{(h_1h_2h_3h_4)}$ give very singular discontinuous cusps in a Wulff plot. The equilibrium morphologies that have been constructed by means of such a Wulff plot for several incommensurately modulated model crystals can be understood in detail. The reason for this is that we have elucidated the influence of several structural aspects on the morphology.

A (satellite) plane is stabilized more when the value of $|\mathbf{f}\cdot\mathbf{b}|$ is larger for important m.b.c.'s intersecting that plane. This is the influence of the direction of the modulation amplitude vector. On the other hand, the amount of stabilization increases with the length of the modulation amplitude vector. Also, the number of (satellite) faces that appear on the morphology increases with the modulation amplitude. Both the length and the direction of the modulation wave vector $\mathbf{q}$ determine the value of $q_1 = \mathbf{q}\cdot\mathbf{b}$ in the $(1+1)$-dimensional embedding of the m.b.c. with bond-chain vector $\mathbf{b}$. The amount of stabilization then depends on this value of q_1 but differs for different $(h_1b_1 + h_2b_2 + h_3b_3, h_4)_s$ planes. This dependence has already been outlined in a previous paper for a sinusoidal modulation (Kremers *et al.*, 1994). In this paper, we have discussed the dependence for a square-wave modulation. One can state that, if the modulation function resembles a square wave, satellite faces are stabilized more with respect to main faces as compared with the case of a sinusoidal wave.

In view of these structural influences on the morphology, we have given a plausible explanation for the appearance of satellite faces on $AuTe_2$ crystals and not on $[(CH_3)_4N]_2ZnCl_4$ crystals.

The authors thank both Professor A. Janner and Professor T. Janssen for their continuous interest, enthusiasm and help. We also acknowledge Dr S. van Smaalen for the very critical and exciting discussions on the subject. This work is part of the research program of the Stichting voor Fundamenteel Onderzoek der Materie (Foundation for Fundamental Research on Matter).

References

BALZUWEIT, K., MEEKES, H. & BENNEMA, P. (1991). *J. Phys. D*, **24**, 203–208.

BENNEMA, P. (1993). *Handbook of Crystal Growth*, edited by D. T. J. HURLE, ch. 7. Amsterdam: Elsevier.

BENNEMA, P., BALZUWEIT, K., DAM, B., MEEKES, H., VERHEIJEN, M. A. & VOGELS, L. J. P. (1991). *J. Phys. D*, **24**, 186–198.

BENNEMA, P. & VAN DER EERDEN, J. P. (1987). *Morphology of Crystals*, Part A, edited by I. SUNAGAWA. Tokyo: Terra Scientific; Dordecht: Reidel.

BENNEMA, P., KREMERS, M., MEEKES, H., BALZUWEIT, K. & VERHEIJEN, M. A. (1993). *Discuss. Faraday. Soc.* **95**, 2–10.

BENNEMA, P., KREMERS, M., MEEKES, H. & VERHEIJEN, M. A. (1994). *Phys. Status Solidi A*, **146**, 13–30.

DAM, B. (1985). *Phys. Rev. Let.* **55**, 2806–2809.

DAM, B. (1986). *Acta Cryst.* B**42**, 69–77.

DAM, B., JANNER, A., BENNEMA, P., VAN DER LINDEN, W. H. & RASING, T. (1983). *Phys. Rev. Lett.* **50**, 849–852.

DAM, B., JANNER, A. & DONNAY, J. D. H. (1985). *Phys. Rev. Lett.* **55**, 2301–2304.

GOLDSCHMIDT, V., PALACHE, C. & PEACOCK, M. (1931). *Neues Jahrb. Mineral.* **63**, 1–58.

HARTMAN, P. & PERDOK, W. G. (1955). *Acta Cryst.* **8**, 49–52, 521–524, 525–529.

HEIJMEN, T. G. A., KREMERS, M. & MEEKES, H. (1994). *Philos. Mag.* **71**, 1083.

HEIJMEN, T. G. A., KREMERS, M., MEEKES, H. & JANSSEN, T. (1995). In preparation.

HERRING, C. (1951). *Phys. Rev.* **82**, 87–93.

HERRING, C. (1953). *Structure and Properties of Solid Surfaces*, edited by R. GOMER & C. S. SMITH. Univ. of Chicago Press.

JANNER, A. & DAM, B. (1989). *Acta Cryst.* A**45**, 115–123.

JANNER, A. & JANSSEN, T. (1977). *Phys. Rev. B*, **15**, 643–658.

JANNER, A. & JANSSEN, T. (1980). *Acta Cryst.* A**36**, 408–415.

JANNER, A., JANSSEN, T. & DE WOLFF, P. M. (1983). *Acta Cryst.* A**39**, 671–678.

JANNER, A., RASING, T., BENNEMA, P. & VAN DER LINDEN, W. H. (1980). *Phys. Rev. Lett.* **45**, 1700–1702.

KREMERS, M., MEEKES, H., BENNEMA, P., BALZUWEIT, K. & VERHEIJEN, M. A. (1994). *Philos. Mag.* B**69**, 69–82.

MADARIAGA, G., ZUÑIGA, F. J., PÉREZ-MATO, J. M. & TELLO, M. J. (1987). *Acta Cryst.* B**43**, 356–368.

SCHUTTE, W. J. & DE BOER, J. L. (1988). *Acta Cryst.* B**44**, 486–494.

SMAALEN, S. VAN (1992). *Mater. Sci. Forum*, **100**, **101**, 173–222.

SMAALEN, S. VAN (1993). *Phys. Rev. Lett.* **70**, 2419–2422.

SMAALEN, S. VAN (1994). Private communications.
SUENO, S., KIMATA, M. & OHMASA, M. (1979). *Modulated Structures*, edited by J. M. COWLEY, J. B. COHEN, M. B. SALAMON & B. J. WUENSCH. *AIP Conf. Proc.* **53**, 333–335.
VAN TENDELOO, G., GREGORIADES, P. & AMELINCKX, S. (1983). *J. Solid State Chem.* **50**, 321–334, 335–361.
VOGELS, L. J. P., BALZUWEIT, K., MEEKES, H. & BENNEMA, P. (1992). *J. Cryst. Growth*, **116**, 397–413.
VOGELS, L. J. P., VERHEIJEN, M. A., MEEKES, H. & BENNEMA, P. (1992). *J. Cryst. Growth*, **121**, 697–708.
WOLFF, P. M. DE, JANSSEN, T. & JANNER, A. (1981). *Acta Cryst.* A**37**, 625–636.

Acta Cryst. (1995). A**51**, 739–746

Maximum-Entropy Analysis of the Cubic Phases of KOH and KOD, NaOH and NaOD

BY KLAUS-DIETER SCHOTTE

Institut Theoretisch Physik, Freie Universität Berlin, Arnimallee 14, 14195 *Berlin, Germany*

URSULA SCHOTTE* AND HANS-JÜRGEN BLEIF

BENSC, Hahn-Meitner Institut, Glienicker Strasse 100, 14109 *Berlin, Germany*

AND ROBERT PAPOULAR

Brookhaven National Laboratory, Upton, New York 11973-5000, *USA*

(*Received* 14 *November* 1994; *accepted* 7 *April* 1995)

Dedicated to Professor W. Prandl on the occasion of his 60th birthday

Abstract

The maximum-entropy method (MEM) for structure determination is applied on the plastically crystalline phases of KOH and KOD characterized by delocalized H^+ or D^+ ions in a simple rock salt structure. The structure factors measured by neutron diffraction already give a consistent picture of the hydrogen distribution by conventional Fourier and modelling methods, which helps to understand the merit of the MEM. Owing to the negative sign of the scattering length of hydrogen, the MEM can, in a limited sense 'model free', separate off the hydrogen density distribution. It is found, however, that the MEM cannot be applied naively for these compounds and reasons are given why the uniform density as *a priori* information has to be given up in the present case. The *a priori* information procedure to be used is discussed. In addition, and perhaps unexpectedly, the deuterium density is also obtained.

1. Introduction

The high-temperature phases of the potassium and sodium hydroxides have sodium chloride structure and are plastic crystals with the H atom moving more or less freely in the vicinity of the O atom (Smit, Dachs & Lechner, 1979; Bleif & Dachs, 1982; Kara, 1982). Obvious questions are: does the OH group behave like a rigid dumb-bell jumping between favourable orientations or is there hydrogen bonding O—H—O or even diffusion of protons to make these compounds ionic conductors (El'kin, 1990)? Are the answers, linked to determining the OH distance, extractable from neutron or X-ray diffraction data?

With conventional methods, the structure determination would be tackled by modelling the anisotropic hydrogen distribution and extracting the Debye–Waller (DW) factors from the fit. For these plastic crystals, the DW factors are very large since the cubic phase is stable only in a temperature region around 550 K. Therefore, there are relatively few measurable reflections and Fourier methods should be reliable, *i.e.* cut-off effects from setting the intensity of unmeasured structure factors to zero should be small. The hydrogen distribution, however, gives rather small contributions to the structure factors and is not easy to separate. The procedure by 'different Fourier analysis' relies heavily on modelling. This, together with the lucky circumstance that all phases are known (they are all +1), makes the system an interesting candidate to test the maximum-entropy method (MEM), recently much propagated as a model-free method for crystallographic structure determination (see, for example, Sakata, Mori, Kumazawa, Takata & Toraya, 1990; Papoular, Prandl & Schiebel, 1992).

It seems one has a chance to find a realistic model-free hydrogen distribution using the fact that hydrogen has a

* Also at Mineralogisch-Petrographisches Institut, Universität Kiel, Germany.